CHAPTER 6

CO_2 application in supermarket refrigeration

CO_2 as a refrigerant has been reported to be used in supermarket application in booster, indirect/cascade and integrated configurations. The improvement in performance of basic CO_2 booster cycle by adoption of various modifications has already been reported in literature for high ambient temperature operation, leading to reduction in both carbon footprint and operational expense. However, the reported studies on CO_2 booster system evaluate the possible modifications mainly based on energetic perspective.

This chapter initially describes the performance comparison of basic CO_2 booster configuration with their possible variants in energy and economic perspectives for operation in warm locations across the globe. The investigated configurations include a standard booster system, a booster system with parallel compressor and its variants, a booster system with flooded low temperature evaporator, a booster system with work recovery expander and a booster with parallel compressor along with flooded low temperature evaporator and work recovery expander. Later, the performance comparison of widely accepted CO_2 booster system with parallel compression is also compared to CO_2 indirect/cascade systems.

Lastly, an integrated cascaded booster configuration is proposed and analyzed for operation in warm climate of India and Middle East. Integrated refrigeration system constitutes both low temperature and medium temperature loads in addition to integration of air-conditioning and heating loads. The performance of proposed all-natural integrated NH_3/CO_2 cascaded booster system is compared to an integrated all-CO_2 multi-jet ejector system based on energy and environmental perspectives. The proposed integrated system seeks to combine the advantages that NH_3 system has for heat rejection at high ambient with that of CO_2 system operating sub-critically.

6.1 Booster and indirect/cascade configurations

Fig. 6.1 shows a standard CO_2 booster system (B1) incorporating both low temperature (LT) and medium temperature (MT) load (Ge et al., 2011). Refrigerant leaving the MT compressor goes to the gas cooler which rejects heat to the ambient air. Expansion of refrigerant at the exit of gas cooler into the intermediate vessel facilitates further cooling of refrigerant before entry into the evaporator while the vapor generated is throttled to the MT evaporator pressure.

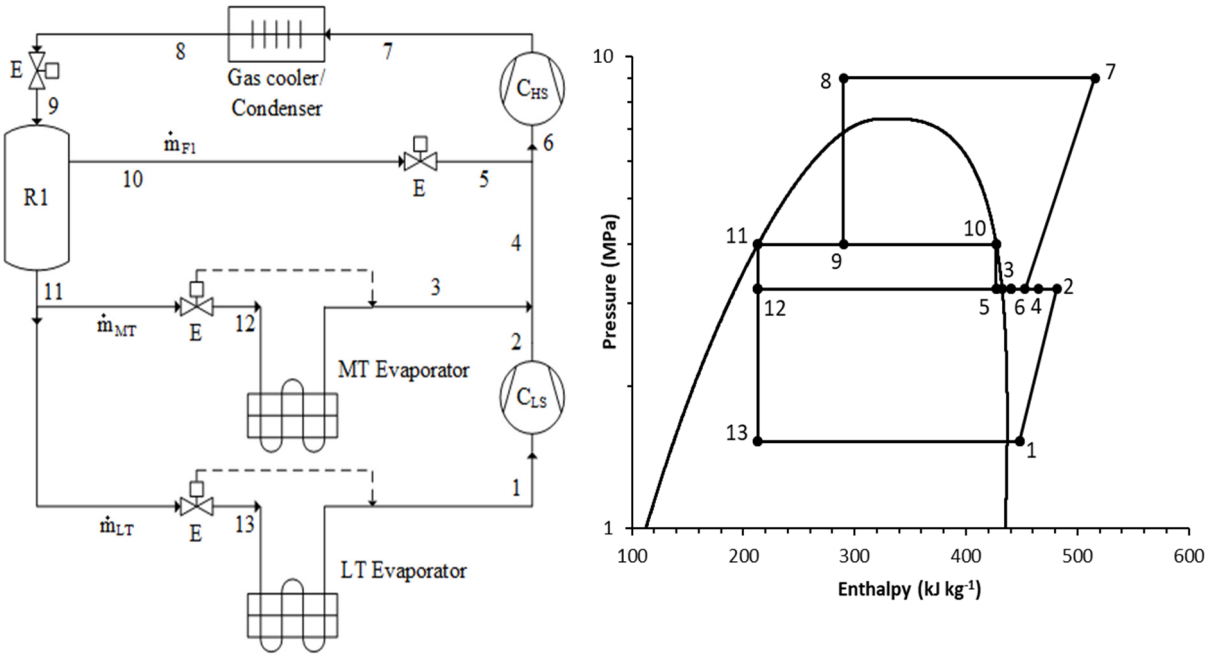

Fig. 6.1 Standard CO_2 booster system (B1)

One simple suggestion for performance improvement of the B1 cycle configuration is adoption of a parallel compressor and thereby reduce load on the high stage compressor, especially for high ambient operation. The extra vapor produced at the intermediate vessel is compressed back to the gas cooler pressure using the auxiliary compressor. The cycle is abbreviated as B2 and is shown in Fig. 6.2. B2 require a control system to simultaneously optimize the gas cooler and intermediate pressure to maximize COP for various ambient temperature. Variants of B2 are also investigated viz booster with compressor inter-cooling (B2a) and booster with flash gas inter-cooling (B2b). In configuration B2a, an inter-cooler is

employed between low stage compressor and high stage compressor. Inter-cooler may be air cooled or water cooled. In flash gas intercooling, configuration B2b, the high temperature CO_2 is flashed in the receiver R1 which leads to cooling of CO_2 as well as flash gas generation.

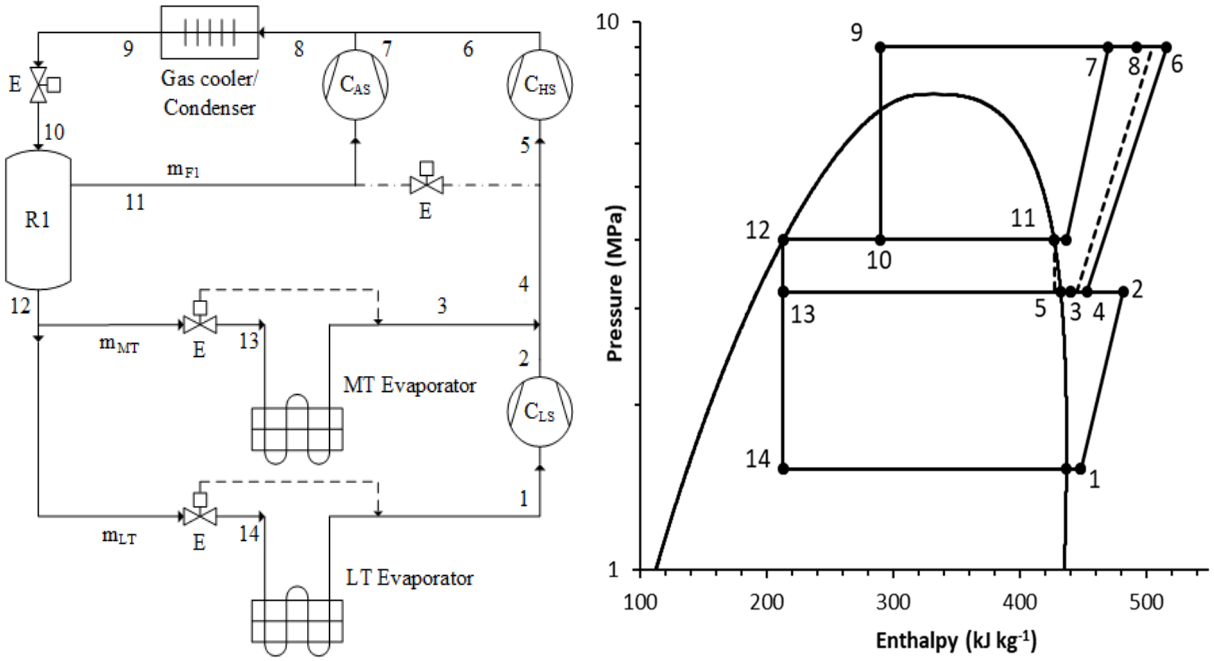

Fig. 6.2 CO_2 booster system with parallel compression (B2)

Next, performance of cycle is analyzed with a flooded LT evaporator as shown in Fig. 6.3. For this, an additional refrigerant receiver (R2) is introduced at LT evaporator pressure. The system is abbreviated as B3. A flooded evaporator operates at a higher temperature than the conventional ones, owing to enhanced heat transfer. However, it requires an additional pump shown as P_{LT} in Fig. 6.3.

Use of work recovery expander in place of expansion valve is the modification proposed next to recover some work to compensate for the compressor power consumption. The proposed B4 cycle is equipped with a work recovery expander over and above B1 configuration as shown in Fig. 6.4.

Next, combination of all the modifications that is parallel compression, flooded LT evaporator and using a work recovery expander in a one single configuration is proposed as shown in Fig. 6.5. The system is abbreviated as B5.

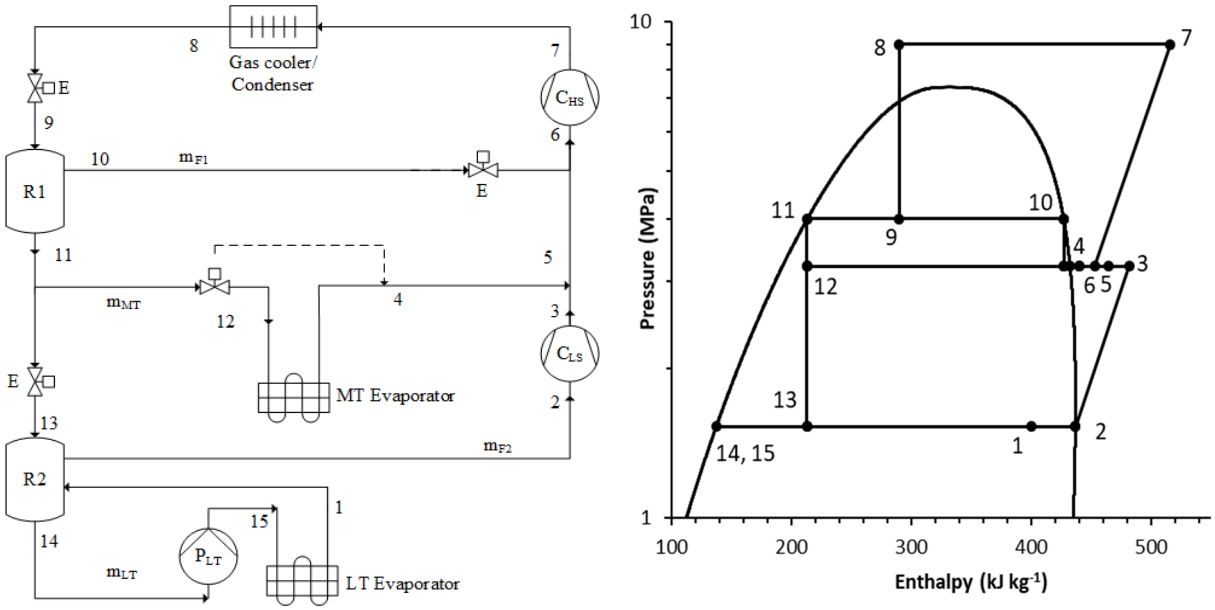

Fig. 6.3 CO_2 booster system with flooded LT evaporator (B3)

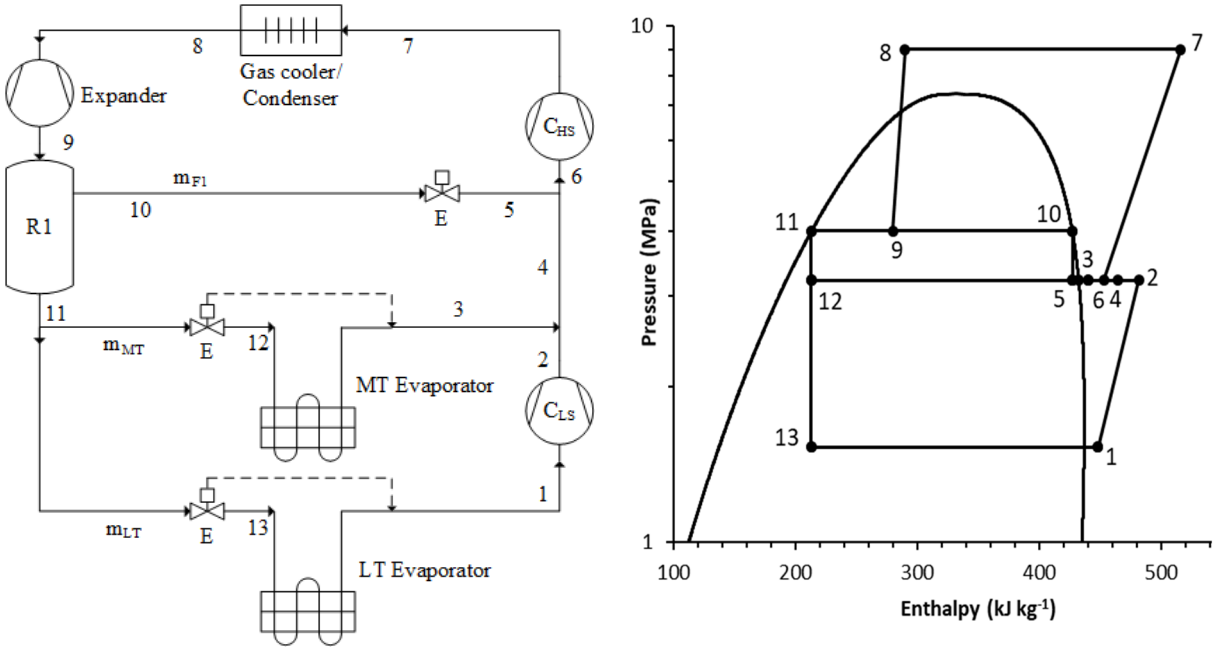

Fig. 6.4 CO_2 booster system with work recovery expander (B4)

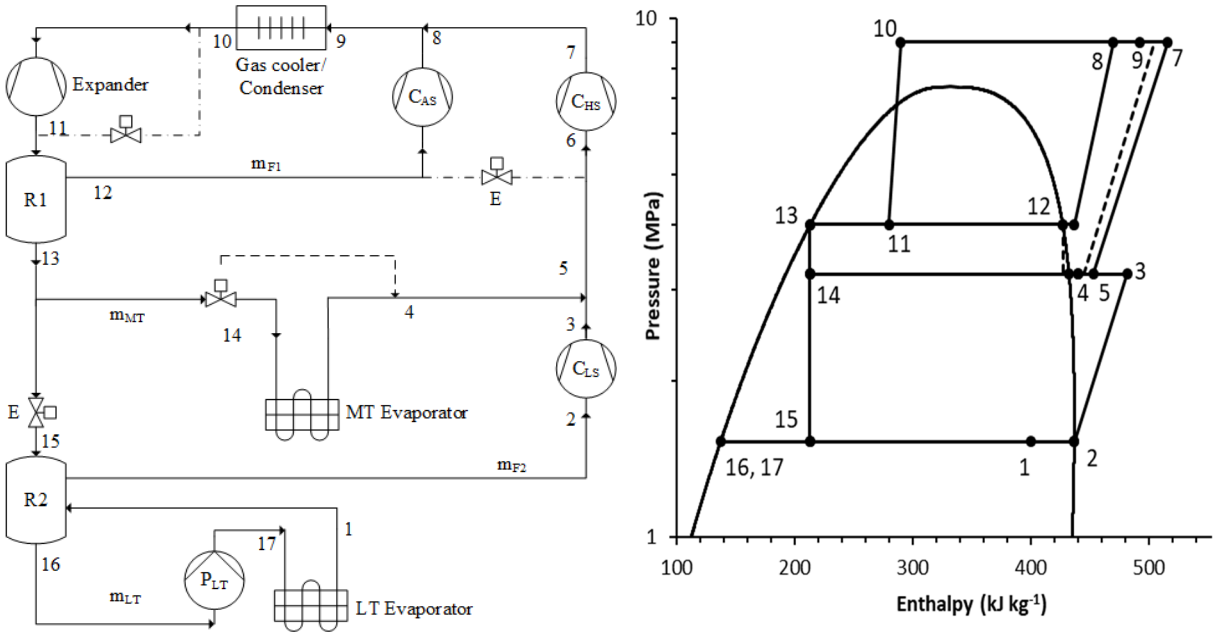

Fig. 6.5 CO_2 booster system with parallel compression along with flooded LT evaporator and work recovery expander (B5)

CO_2 is also a promising secondary working fluid since it offers reduced pump's work and pipes' size and good heat transfer characteristics. Furthermore, the high vapour density of the R744 allows decreasing the inner diameters, while its high saturation pressure permits reducing the compressor's size. In the indirect solutions, CO_2 operates at sub-critical running modes, removing the technical and economic challenges due to very high operating pressures.

Moreover, the secondary loop systems with CO_2 as the secondary fluid can counterbalance the drop in COP caused by the additional heat transfer level and the pump's power. The combined CO_2/R1234ze(E) secondary/cascade configurations shown in Fig. 6.6 are selected as additional alternatives to booster as well as to a R404A direct multiplex expansion (DXS) system (abbreviated as R). R1234ze(E) and R744 are employed as the primary and secondary fluid, respectively.

The main difference between CSC (Fig. 6.6 (a)) and FCSC (Fig. 6.6 (b)) is that the former has flooded evaporators only in the MT circuit, whereas FCSC uses them in both the

MT loop and the LT one. The enhancement of the refrigerant-side heat transfer related to this type of heat exchangers allows increasing the corresponding evaporating temperature.

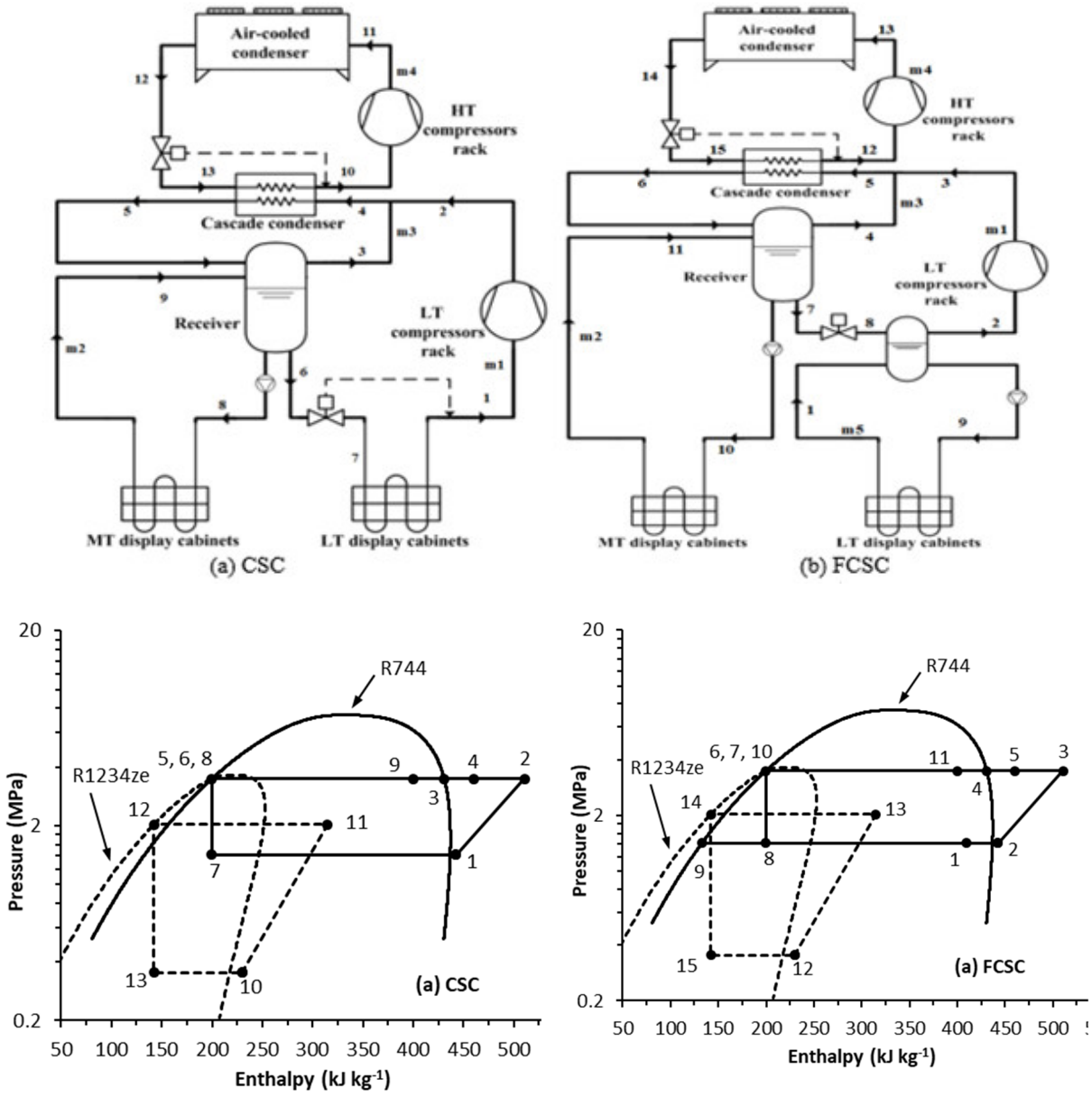

Fig. 6.6 Combined CO_2/R1234ze(E) secondary/cascade configurations

6.1.1 Modelling

Thermodynamic models are developed assuming steady state operation, no heat transfer or pressure loss in piping and components and isenthalpic expansion in expansion valves. Simulation is conducted in MATLAB and the thermo-physical properties of refrigerant are invoked using REFPROP 9.0. The model developed for B1 is validated against

published field data (Sawalha et al., 2015), as shown in Fig. 6.7. For the model validation, MT evaporator and LT evaporator temperatures are taken as -7˚C and -31.5˚C respectively. The high stage and low stage compressor efficiency are 70% and 55% respectively. Evaporator internal superheat at both MT and LT are assumed 7˚C. External evaporator superheat at MT and LT are taken as 8˚C and 13˚C respectively. The maximum deviation between predicted and experimental COP is found to be 5.21%.

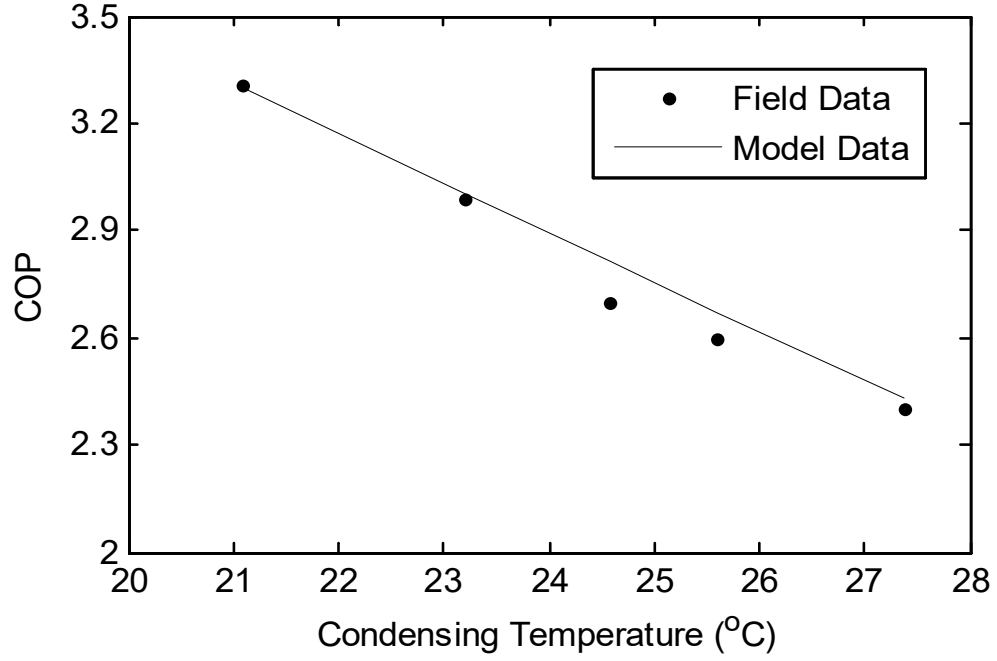

Fig. 6.7 Comparison of COP obtained from thermodynamic model with field data extracted from Sawalha et al., (2015)

6.1.1.1 Ambient conditions

Across the world, four cities with high population density and warm climate are chosen for analysis. These are New Delhi, Teheran, Phoenix and Seville. Hourly averaged year round ambient temperature variation for the selected locations are obtained (TRNSYS 17) as shown in Fig. 6.8. It is observed that while the average ambient temperature in a year for New Delhi is higher than 25°C for about 57.5% of time, for Seville, Teheran and Phoenix the same is for about 21%, 29% and 44% of time respectively.

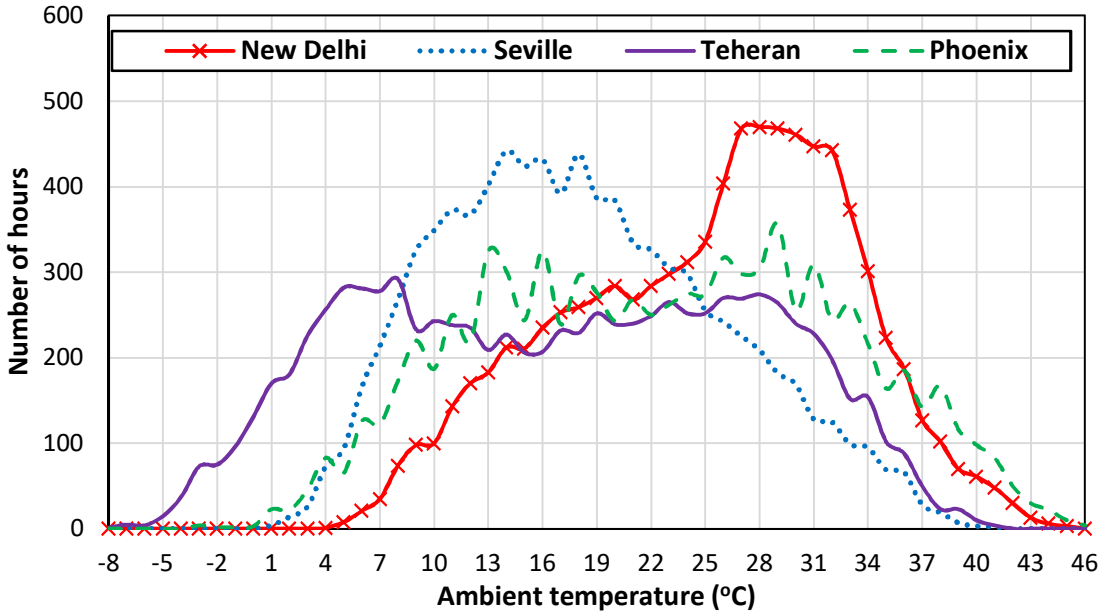

Fig. 6.8 Year-round ambient temperature variation for selected locations

6.1.1.2 Display cabinets

The MT refrigeration load is taken as two times that of LT load for supermarkets as per literature (Girotto et al., 2004). An average sized supermarket is assumed having LT and MT side loads as 65 kW and 120 kW respectively (Sharma et al., 2014a). The medium temperature load is divided over multiple 5 kW cabinets, each having two parallel 72 m length pipe with 15.9 mm diameter. Each freezing cabinet of 2.5 kW capacity is assumed, having single coil of 72 m length and diameter of 12.7 mm (Cabrejas, 2006).

The approach temperatures and change of air temperatures across the display cabinets are assumed based on the literature (Sawalha, 2008a, 2008b). Referring to Fig. 6.9, for MT DX evaporator, the design product temperature is assumed as 3˚C, the air inlet temperature is taken as 3˚C higher than warmest product temperature and the air temperature difference across the heat exchanger is assumed as 7˚C (Sawalha, 2008a). The approach temperature for MT DX evaporator is taken as 5˚C and the superheat assumed is 9˚C. The approach temperature for MT flooded evaporator is taken as 2˚C. For LT evaporator, the design product temperature is assumed as -18˚C, the approach temperature is taken as 2˚C for flooded type and 5˚C for DX, the superheat of 9˚C is taken for DX type, the warmest product

temperature is taken 2.5˚C higher than the air inlet temperature and the air temperature difference across the heat exchanger is assumed as 7.5˚C (Sawalha, 2008a, 2008b). For simplicity, pressure drop within the evaporator is not included while estimating evaporation temperatures for display cabinets. The calculated evaporation temperature for DX type MT and LT evaporator are -8˚C and -34.5˚C respectively. For the LT flooded evaporator, the calculated evaporation temperature is -30˚C, which leads to 4.5˚C increment in evaporation temperature as compared to that of LT DX evaporator. Evaporation temperature for MT flooded evaporator computed is -5^{o}C.

Circulation ratio, referring to LT flooded evaporator, is defined as the actual mass flow of refrigerant to the mass flow required for the complete evaporation. As per the study by Sawalha, (2008a), the heat transfer characteristics for CO_2 is reported to increase with increase in circulation ratio. However, the pressure drop associated is also found to increase. Further, the rate of increase in pressure drop is found higher than that of heat transfer coefficient. So, to define an optimal circulation ratio for any system, two important consideration suggested by (Sawalha, 2008c) are followed and these are (a) The circulation ratio should not be very high to avoid large pressure drop and (b) The circulation ratio should not be very low in order to avoid dry out at the evaporator outlet and should be sufficient enough to sustain load fluctuations. Hence, a circulation ratio of 2.5 in the LT evaporator and 1.5 in the MT evaporator is used in this study. Pressure calculations across the flooded evaporators in this paper are adopted as suggested by Sawalha and Palm, (2003) and a pump efficiency of 50% is assumed.

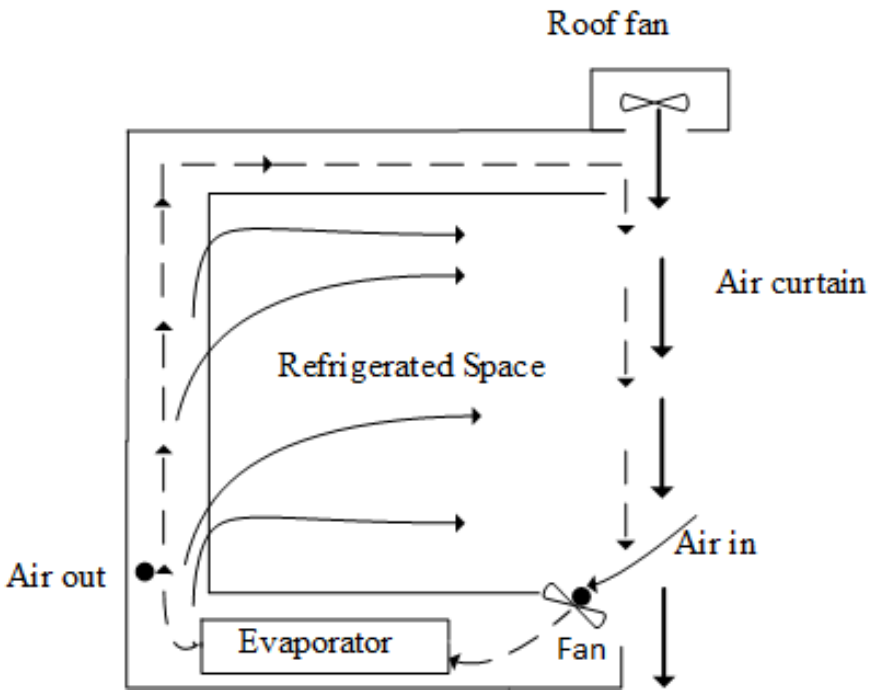

Fig. 6.9 Display cabinets with air curtain

6.1.1.3 Operating conditions

The systems are analyzed for a wider range of ambient temperature ranging from -8°C to 46°C covering year-round ambient condition of selected locations. The optimum high side pressure for a CO_2 cycle with an expansion valve is controlled by adjusting the expansion valve. Whereas, in a cycle with an expander, the high side pressure is optimized by manipulating the mass flow rate through the expander. The expander mass flow rate can be varied by varying the expander speed or changing the displacement volume. Huff and Radermacher (2003) evaluated various possible options for manipulating high side pressure in expander system. Based on their analysis, it is suggested that the expander speed is the only plausible control variable in the expander system. The control strategy adopted to control high side pressure also affects the expander efficiency and considering the same, the isentropic efficiency of the expander for present study, is assumed as a function of pressure ratio. The isentropic efficiency is computed using equation (6.1) (Dai et al., 2017).

$$\eta_{exp} = 1.0094 - (0.0504 \times p_r) \quad (6.1)$$

As suggested by Sharma et al., (2014a), intermediate pressure for the B1 is fixed at 3.5 MPa, however, this will affect the optimal working of the B1 (Cabello et al., 2012). For systems employing parallel compressors, the intermediate pressure is optimized based on the varying ambient temperature. The operating parameters are consolidated in Table 6.1.

Correlations provided by the Gullo et al., (2016a) as shown in Table 6.2, are adopted for the compressors isentropic efficiencies for booster configurations. The adopted correlations are obtained using Dorin Software, which respects technological constraints and thus limits the maximum compressor discharge pressure to 10.6 MPa. The compressor global efficiencies for indirect and baseline configurations are computed from the correlations listed in Table 6.3. The applied limit on the compressor discharge pressure and temperature, affects the COP, especially at high ambient temperature. Firstly, the system cannot be operated at optimum gas cooler pressure (greater than 10.6 MPa) at high ambient temperatures, resulting in drop in performance. Secondly, with increase in ambient temperature, the flash gas generation increases for the system held at constant gas cooler pressure, which brings down the COP.

Table 6.1 Operating parameters of the investigated systems

MT/LT load	120/65	kW
Minimum condensing temperature for CO_2/indirect systems	9/25	°C
Approach temperature of the CO_2 condensers/gas cooler	3/2	°C
Condenser approach temperature for indirect systems	10	°C
Approach temperature of the cascade condensers for indirect systems	2	°C
DX MT/LT evaporating temperature	-8/-34.5	°C
Flooded MT/LT evaporating temperature	-5/-30	°C
Superheating	5	°C
Degree of subcooling in the sub-critical mode I and II	2	°C
Circulation ratio for LT flooded evaporator (CR)	2.5	
Intermediate vessel (R1) pressure for B1	3.5	MPa
Maximum allowable gas cooler pressure	10.6	MPa

Table 6.2 Correlations for compressor efficiencies for booster configurations

Compressor	Isentropic efficiency
LS	$\eta_{LS} = (-0.0012 \times (P_{MT}/P_{LT})^2) - \left(0.0087 \times (P_{MT}/P_{LT})\right) + 0.6992$
HS (sub-critical)	$\eta_{HS} = (-0.1155 \times (P_{cond.}/P_{MT})^2) + \left(0.5762 \times (P_{cond.}/P_{MT})\right) - 0.0404$
HS (transition)	$\eta_{HS} = \left(-0.1155 \times \left(P_{gc/cond.}/P_{MT}\right)^2\right) + \left(0.5762 \times \left(P_{gc/cond.}/P_{MT}\right)\right) - 0.0404$
HS (trans-critical)	$\eta_{HS} = \left(-0.0021 \times \left(P_{gc}/P_{MT}\right)^2\right) - \left(0.0155 \times \left(P_{gc}/P_{MT}\right)\right) + 0.7325$
AS (sub-critical)	$\eta_{AS} = (-0.172 \times (P_{cond.}/P_{R1})^2) + \left(0.7095 \times (P_{cond.}/P_{R1})\right) - 0.0373$
AS (transition)	$\eta_{AS} = \left(-0.172 \times \left(P_{gc/cond.}/P_{R1}\right)^2\right) + \left(0.7095 \times \left(P_{gc/cond.}/P_{R1}\right)\right) - 0.0373$
AS (trans-critical)	$\eta_{AS} = \left(-0.0788 \times \left(P_{gc}/P_{R1}\right)^2\right) + \left(0.3708 \times \left(P_{gc}/P_{R1}\right)\right) + 0.2729$

Table 6.3 Compressor global efficiencies of indirect and baseline systems

Compressor	Efficiency as a function of RP
R, LT	*-0.0075(RP²) + 0.0652(RP) + 0.5609*, RP=pressure of condenser/pressure of LT evaporator
R, MT	*-0.0004(RP²) - 0.0021(RP) + 0.6989*, RP=pressure of condenser/pressure of MT evaporator
CSC and FCSC, second. fluid circuit	*+0.0111(RP²)-0.0793(RP)+ 0.8030*, RP=pressure of cascade condenser/pressure of LT evaporator
CSC and FCSC, primary fluid circuit	*-0.0028(RP²) + 0.0419(RP) + 0.5305*, RP=pressure of condenser/pressure of cascade condenser

6.1.1.4 Control strategy

Control strategy suggested by Gullo et al., (2016a) for booster configurations, is adopted in the present study as shown in Fig. 6.10. Four operating modes are identified for the full range of ambient temperatures in the sample cities. For temperature, less than 4°C or mode I, all investigated systems operate in sub-critical mode with a fixed minimum allowable condenser temperature of 9°C. For temperature, greater than 4°C up to 17°C, sub-critical mode II, the condenser temperature is kept 3°C higher than the ambient temperature. For both

the sub-critical mode, I and II, sub-cooling of 2°C is maintained by adjusting the condenser fan power. The shift from subcritical mode II to transition mode III occurs at ambient temperature greater than 17°C, where the condensing pressure and condensing temperature are governed by equation (6.2) and equation (6.3) respectively. The full trans-critical operation, mode IV, commences at temperature greater than 28°C, where the gas cooler outlet temperature is held at 2°C higher than the ambient, while the gas cooler pressure is optimized dynamically. The auxiliary compressor and work recovery expander start operating at the onset of transition region, i.e. mode III. At ambient temperatures below 18°C, the performance of B2 and B4 is similar to that of B1, while B3 performs same as B5.

$$T_{gascooler/condenser}(^{o}C) = (0.9 \times T_{amb}) + 4.7 \quad (6.2)$$

$$P_{gasccoler/condenser}(kPa) = \left(166.33 \times T_{gascooler/condenser}\right) + 2676.3 \quad (6.3)$$

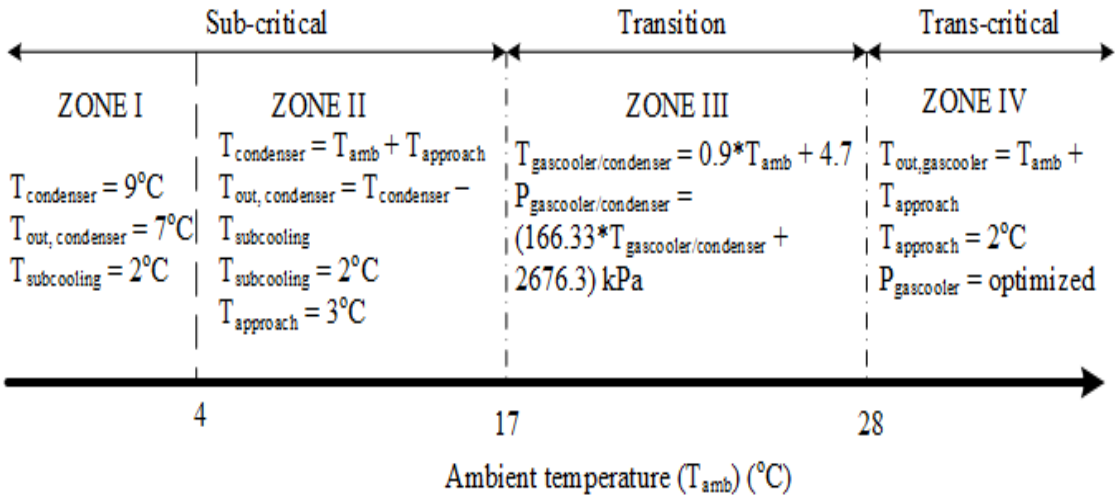

Fig. 6.10 Control strategy for investigated booster configurations

6.1.2 Energy analysis of booster configurations

In this section following parameters are compared for all investigated cycles: COP, optimal gas cooler pressure, receiver pressure and flashed mass flow rate. Power consumed by compressors and the pump for flooded evaporator, collectively forms the total power consumption as given by equation (6.4). Fan power consumption in heat exchanger is neglected as it is a small fraction of the other consumptions and nearly constant for all

investigated configurations. COP is computed as the ratio of the sum of total cooling capacity (MT and LT) to the sum of the total power input, as given by equation (6.5).

$$\dot{W}_{total} = \dot{W}_{LS} + \dot{W}_{HS} + \dot{W}_{AS} + \dot{W}_{pump} - \dot{W}_{wr} \tag{6.4}$$

$$COP = \frac{(\dot{Q}_{MT} + \dot{Q}_{LT})}{\dot{W}_{total}} \tag{6.5}$$

Optimal pressure for gas cooler and receiver corresponds to the pressure where the system is operated at maximum COP for a given ambient condition. To investigate a new dimensionless parameter, Alpha, is formulated. Alpha is defined as the ratio of flashed mass flow rate of vapor at receiver (R1) to the total mass flow rate of the refrigerant in the system at various operating conditions. Comparison of performance of B1, B2, B3, B4 and B5 in terms of COP at various ambient temperature is shown in Fig. 6.11. For ambient below 4°C i.e. subcritical mode I, the COP of all five system remains constant regardless of variation in ambient temperature.

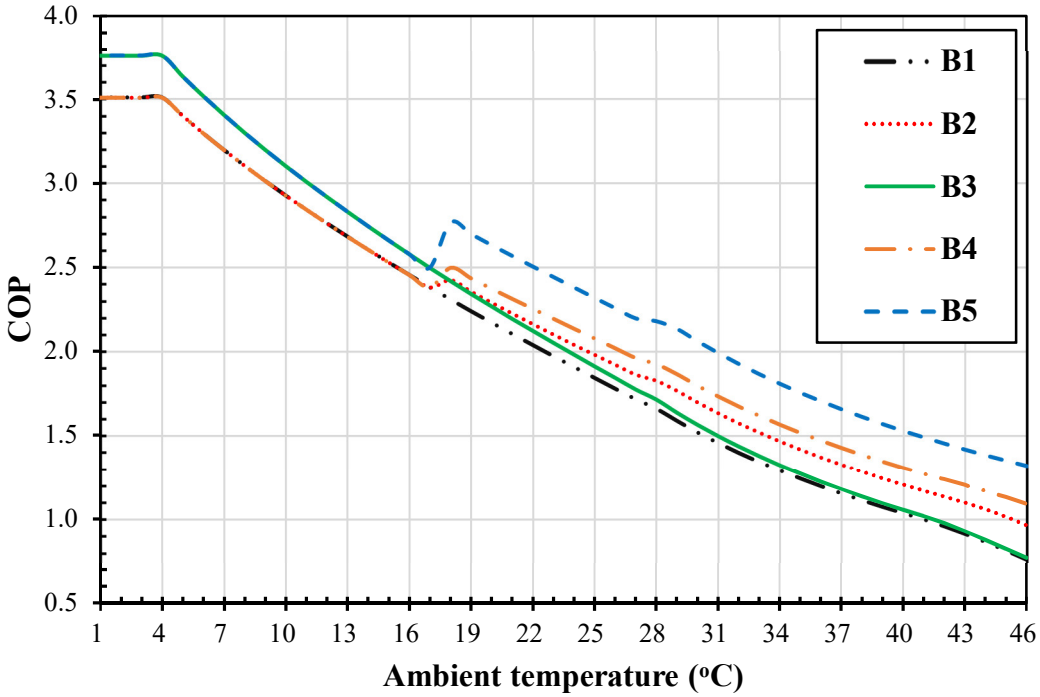

Fig. 6.11 COP of investigated booster systems at various ambient temperature

This is because the condensing temperature is fixed at 9ºC, with sub-cooling of 2ºC. At the onset of sub-critical mode II, the COP of all configurations is found to be inversely proportional to the change in ambient temperature. However, the magnitude of COP for system with flooded evaporator is higher. Performance of B1 is similar to that of B2 and B4 while COP for B3 and B5 are equal for mode I and II. At the onset of transition mode III, a sharp increase in COP is observed for B4 and B5 due to the commencement of work recovery by expander. Similar, behavior with a lower magnitude is observed for B2 owing to removal of flash gas by an auxiliary compressor. The COP for all systems have a negative trend with increase in ambient temperature in mode IV. B5 followed by B4, B2 and B3 are found to be better solution over and above B1, specially for warm climatic operation. The improvement in performance of system employing work recovery expander eventually increases with increase in ambient temperature. This may be attributed to the increase in the work recovery potential at high ambient temperatures. For instance, at ambient temperature of 30ºC, the improvement in COP of B4 and B5 over B1 is found to be 18.3% and 35.6% respectively. While, at ambient temperature of 46ºC, the improvement in performance of B4 and B5 over B1 is 43.5% and 73.5% respectively. Such high percentage of relative improvement in performance of modified systems at high ambient temperature may be attributed to the limit set on the maximum allowable gas cooler pressure. Comparison of performance of variants of B2 viz B2a and B2b in terms of COP depicts parallel compression followed by flash gas removal to be better option. While flash gas inter-cooling to be better for the cold climatic conditions. The difference in COP for system with and without flooded evaporator eventually decreases with increase in ambient temperature as noticeable from Fig. 6.11. The trend for the COP for the LT flooded evaporator is found consistent with the results reported by Sawalha, (2008a). At the highest investigated ambient temperature of 46ºC the

COP for B1, B2, B3, B4 and B5 are found to be 0.760, 0.964, 0.768, 1.091 and 1.319 respectively.

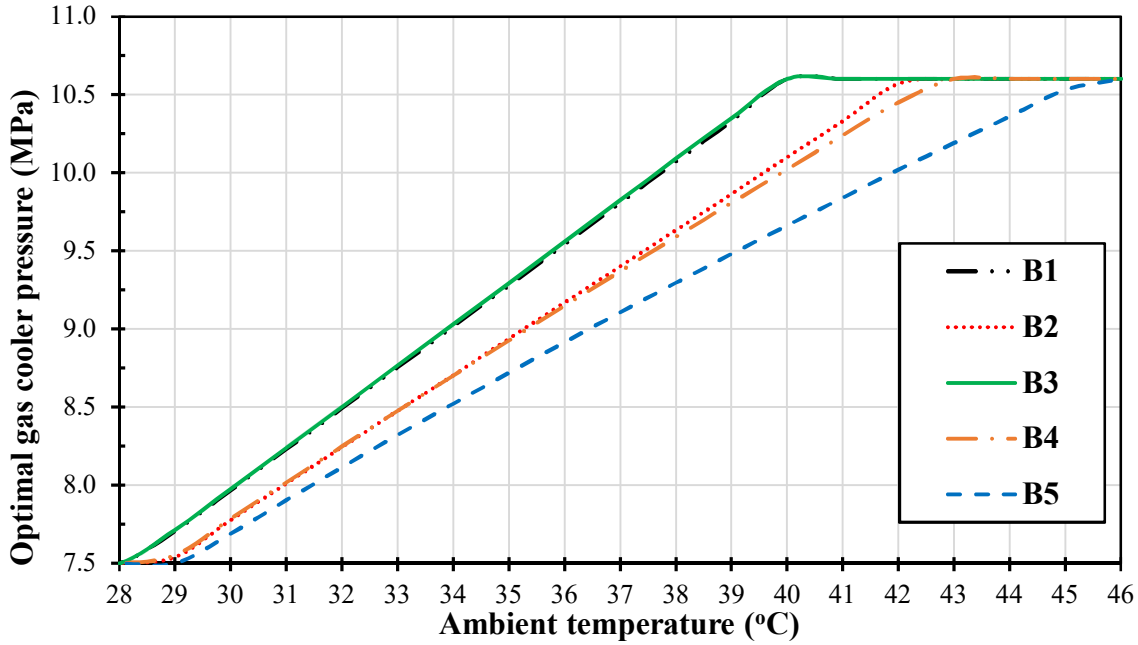

Fig. 6.12 Optimal gas cooler pressure of booster systems at various ambient temperature

Fig. 6.12 shows optimal gas cooler pressure for all five systems in mode IV, corresponding to the best possible COP. As expected, the optimized gas cooler pressure shows an almost linear rise with increase in ambient temperature. B1 is found to operate at higher gas cooler pressure. At ambient temperature of 40°C, B1 reaches the maximum allowable gas cooler pressure of 10.6 MPa considered as upper limit in the simulation. The behavior of optimal gas cooler pressure for B3 is found to be similar to that of B1. The lowest operating gas cooler pressure is observed for B5 owing to the combination of parallel compression and work recovery. This implies that adoption of B5 is more suitable at higher ambient temperature. The lower value of optimal gas cooler pressure for B5 implies better compressor life and improvement in overall system performance.

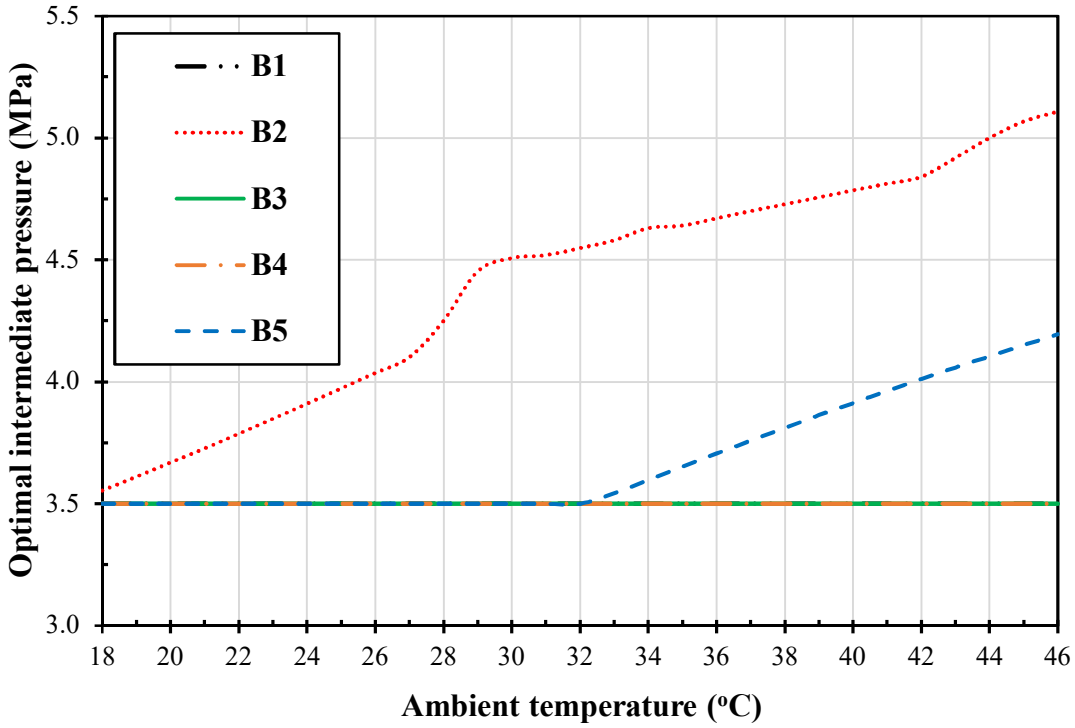

Fig. 6.13 Optimal receiver (R1) pressure of booster systems at various ambient temperature

The optimal receiver pressure for all investigated configurations operating in mode III and mode IV are shown in Fig. 6.13. Note that the receiver pressure for B1, B3 and B4 are kept constant at 3.5 MPa throughout the simulation. B5 is found to have lower optimal inter stage pressure compared to that of B2. The work recovery expander in B5 operates between gas cooler pressure and the receiver pressure. So, lower receiver pressure implies comparatively higher power recovery, however, at the same time, the power required by the auxiliary compressor increases. Subsequently, the optimal receiver pressure for B5 is a compromise between the power recovered in the expander and the power required by the compressor. Further, adoption of additional receiver at LT evaporator pressure (R2) in B5, leads to increase in mass flow rate, which in turn also contributes to the rise in the receiver pressure. For B2 there is no such work recovery, therefore, this system operates at comparatively higher receiver pressure to have lower compressor power.

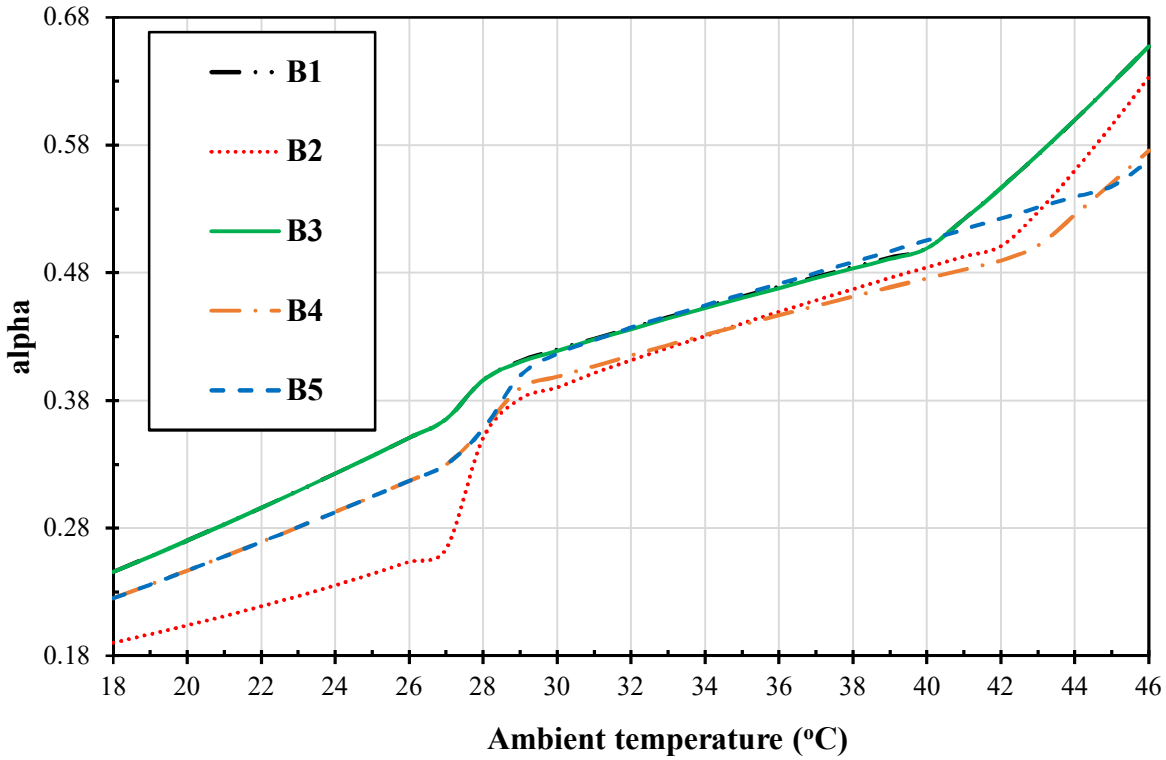

Fig. 6.14 Ratio of flashed mass flow rate at R1 to the total mass flow rate (α)

Variation in flash gas generated as a fraction of total mass flow rate (α) at optimal receiver pressure for all five systems are shown in Fig. 6.14. With increase in ambient temperature, the α at receiver R1 increase while that at receiver R2 (not shown in figure) decreases due to the fixed LT evaporator pressure. For mode III, having gas cooler outlet state governed by equation 6.2 and 6.3 and same for all systems, B1 and B3 are found to have comparably higher α. This may be attributed to the higher flash gas generation. B2 shows receiver pressure (R1) higher than 3.5 MPa, which results in lower α. Further, in zone III, B4 and B5 have slightly lower α as compared to B1 and B3 due to the polytrophic expansion of refrigerant in the expander, which leads to decrease in quality of refrigerant at the inlet of receiver R1 and ultimately lower flash gas generation. In zone IV, as the gas cooler pressure reaches the maximum allowable limit of 10.6 MPa, a sudden rise of α is observed for all the investigated systems. This is since at fixed gas cooler pressure, the flash gas generation increase with increase in ambient temperature.

The annual energy savings for investigated systems over and above B1 is plotted in Fig. 6.15. It is observed that the annual energy savings for B5 is highest followed by B4, B2 and B3. Annual energy savings for B3 over and above B1 is found least and nearly same for all the cities investigated. Work recovery expander unit has the highest share in performance improvement of B5, followed by parallel compression and flooded evaporator. Further, for B5, the energy savings at New Delhi is comparatively higher than to other cities due to a larger share of time period in transition modes III and trans-critical mode IV. A similar trend but overall lower value is obtained for the other two systems B4 and B2.

For Seville and Teheran, B4 and B5 operates majority of the time in sub-critical and transition mode, leading to lower annual savings over and above B1. Annual energy savings in Phoenix is comparable to that in New Delhi as in Phoenix ambient temperature persists above 37^{o}C for higher number of hours. The maximum annual energy savings for configuration B5 over and above configuration B1 in New Delhi, Seville, Phoenix and Teheran are 207.69 MW· hr, 112.45 MW· hr, 182.05 MW· hr and 125.01 MW· hr respectively.

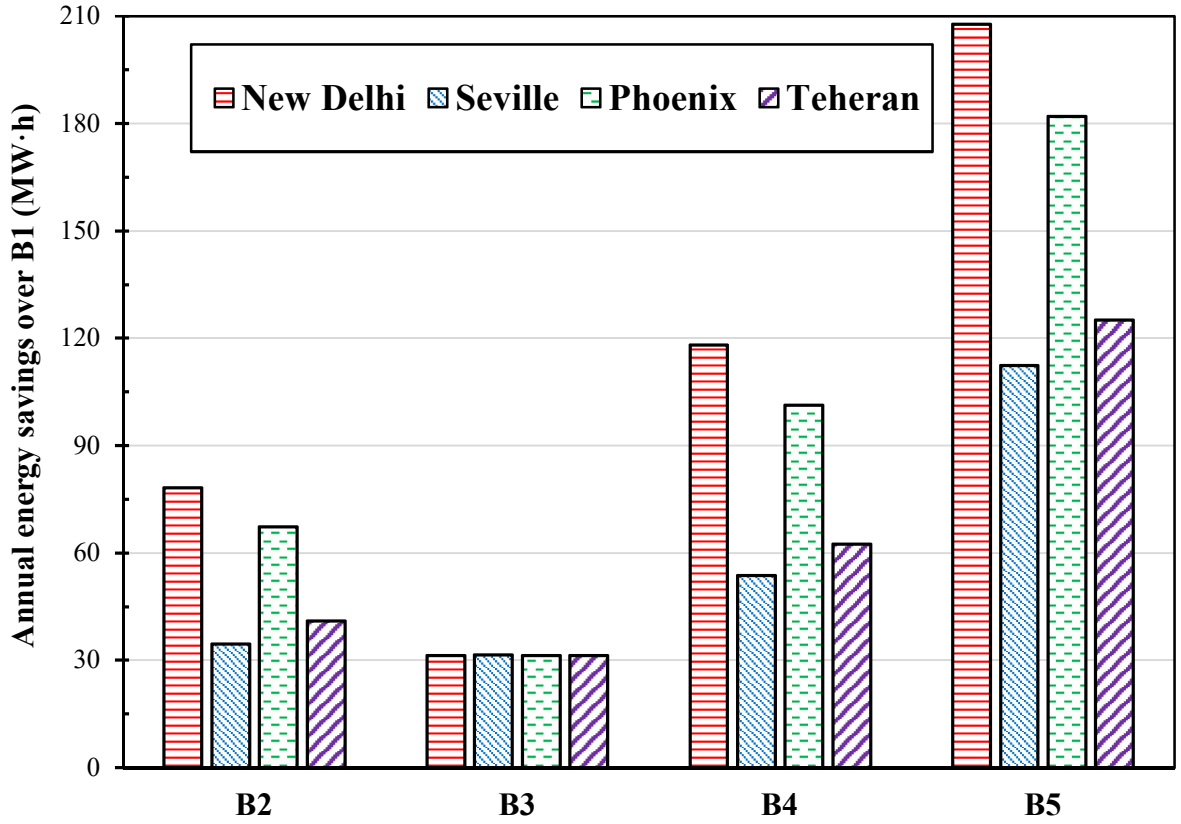

Fig. 6.15 Annual energy savings over and above B1 for booster systems investigated

6.1.3 Economic analysis of booster configurations

Limited scale economic analysis is conducted in this section in support of augmentations made to B1 configuration to obtain B2 to B5. Investment recovery time and total money saved in the lifetime are compared. The additional investment recovery time (AIRT) is calculated using equation (6.6).

$$AIRT = \frac{Increase\ in\ capital\ cost}{ES \times unit\ cost\ of\ electricity} \tag{6.6}$$

Various assumptions made for solving equation (6.6) are as following:

- The capital cost of the CO_2 compressor is expressed as a function of power consumed at design temperature (Fazelpour and Morosuk, 2014), as in equation (6.7).

$$C_{Compressor,CO_2} = 10167.5 \times \left(\dot{W}\right)^{0.46} \tag{6.7}$$

- The motor for driving the compressor contributes to about 50 % of the total compressor cost while remaining is for the impeller mechanism (Subiantoro and Tiow, 2013). The motor part is not required for the expander application. Also, the size of the expander is expected to be less than that of compressor in the cycle owing to reduced displacement volume. However, there will be additional cost for mechanical to electrical energy conversion unit. Cost of the expander along with energy conversion unit is, therefore, assumed to be equal to the compressor cost.
- The purchase cost of the heat exchanger is calculated as a function of required heat transfer area (Mosaffa et al., 2016), expressed by equation (6.8).

$$C_{HX} = 1397 \times (A)^{0.89} \tag{6.8}$$

- For flooded evaporator, additional pump is required and its purchase cost is assumed as $\$1000 \cdot kW^{-1}$ (Loh et al., 2002). Receiver and expansion valve costs are assumed as \$1000 and \$100 respectively (Gullo et al., 2015).
- The cost of installation of additional equipment like control system and piping is assumed to be equal to 15% of the total purchase cost of the system (Fazelpour and Morosuk, 2014).
- The cost of electricity consumption is 120 $\$ \cdot MW \cdot hr^{-1}$ for Delhi, 170 $\$ \cdot MW \cdot hr^{-1}$ for Phoenix, 190 $\$ \cdot MW \cdot hr^{-1}$ for Teheran, 227.3 $\$ \cdot MW \cdot hr^{-1}$ for Seville (Energy Use Calculator, 2016).
- The design temperature of 43.8ºC, 43.5ºC, 38.7ºC and 39.8ºC are taken for New Delhi, Phoenix, Teheran and Seville respectively (ASHRAE, 2014). Interest rate on borrowed capital is neglected for the analysis.

The results from economic analysis are summarized and represented in Table 6.4. The deliverables include purchase cost of equipment, additional investment recovery time and the money saved in the lifetime of the system. It is noticeable from the Table 6.4 that the cost of

compressor, gas cooler and expander constitute the major cost of the system. The additional investment recovery time is found lowest for B3 irrespective of the location (Table 6.4).

However, the total money saved during the lifetime of system is found lower. On the other hand, additional investment recovery time is found higher for B4 and B5, while the total money saved over the lifetime is higher. These are attributed to two factors, firstly, to lower initial cost of B3 vs savings and secondly, to superior annual energy savings for B4 and B5. The performance of B2 declines at high ambient temperature due to the increase in flash gas generation, leading to lower annual energy savings and higher additional investment recovery time as noticeable in Table 6.6.

The additional investment recovery time and money saved during the life time of system greatly depends on local electricity tariff and annual energy savings. City of Phoenix depicts lowest recovery time and corresponding superior money savings owing to comparably higher annual energy savings and moderate electricity tariff values. In contrast, New Delhi, despite having higher annual energy savings, the recovery time is longer, and the cumulative money saved is lower due to lower electricity tariff. For Teheran, the recovery time and money saving are inferior due to both lower annual energy savings and moderate electricity tariff.

The sensitivity of annual energy savings and additional investment recovery time for B5 on local electricity tariff and assumed isentropic efficiency of work recovery expander for the city of New Delhi is assessed and the result is presented in Fig. 6.16. For a local electricity tariff value, reduction in additional investment recovery time is noticeable with increase in the isentropic efficiency of expander. The reduction is found more prominent at lower local electricity tariff. The additional investment recovery time shows a non-linear trend with respect to local tariff for an isentropic efficiency. The slope of recovery time is steeper at lower tariff values as compared to that at higher tariff values.

Table 6.4 Economic analysis of booster investigated systems

Location	Cycle	LS compressor cost ($)	HS compressor cost ($)	AS compressor cost ($)	Gas cooler cost ($)	LT evaporator cost ($)	MT evaporator cost ($)	Total cost ($)	Cost over and above BC1	ES over and above B1 (MW·hr)	Electricity tariff ($·MW·h^{-1})	AIRT (year)	Money saved in lifetime of system ($)
New Delhi	B1	35433.3	112035.5	—	71742.3	25842.3	44597.4	335398.4	—	—	—	—	—
	B2	38200.6	84312.4	58697.8	79584.3	25842.3	44597.4	383220.2	47821.7	78.3	120.0	5.1	140917.45
	B3	31998.5	112035.5	—	72948.3	25842.3	44597.4	337835.5	2437.1	31.3	120.0	0.6	56413.80
	B4	35433.3	104496.5	—	61492.4	25842.3	44597.4	386278.4	50879.9	118.1	120.0	3.6	212502.85
	B5	32991.0	78943.4	62032.3	69598.7	25842.3	44597.4	434743.1	99344.6	207.7	120.0	4.0	373856.98
Teheran	B1	35433.3	100237.4	—	62418.4	25842.3	44597.4	311108.1	—	—	—	—	—
	B2	37682.3	80002.1	49527.4	70725.1	25842.3	44597.4	356933.0	45824.9	40.9	190.0	5.9	116580.16
	B3	31986.4	100109.8	—	63482.3	25842.3	44597.4	313221.0	2112.9	31.3	190.0	0.4	89105.19
	B4	35433.3	95955.9	—	59306.9	25842.3	44597.4	366638.9	55530.8	62.4	190.0	4.7	177981.59
	B5	32564.9	74562.4	55680.6	66167.3	25842.3	44597.4	410659.9	99551.8	125.0	190.0	4.2	356288.65
Phoenix	B1	35433.3	111080.0	—	70816.9	25842.3	44597.4	333235.4	—	—	—	—	—
	B2	38151.1	84203.0	57757.3	78156.9	25842.3	44597.4	380314.3	47078.9	67.3	170.0	4.1	171551.81
	B3	31998.5	111080.0	—	72024.9	25842.3	44597.4	335674.7	2439.3	31.3	170.0	0.5	79690.94
	B4	35433.3	103856.9	—	60985.9	25842.3	44597.4	384345.8	51110.4	101.3	170.0	3.0	258412.16
	B5	32967.5	78749.1	61497.9	69192.0	25842.3	44597.4	432795.7	99560.3	182.1	170.0	3.2	464228.62
Seville	B1	35433.3	102284.1	—	62589.4	25842.3	44597.4	313658.4	—	—	—	—	—
	B2	37742.5	81159.0	51045.6	71245.4	25842.3	44597.4	360677.1	47018.6	34.6	228.0	6.0	118429.06
	B3	31998.5	102159.5	—	63614.2	25842.3	44597.4	315743.8	2085.3	31.5	228.0	0.3	107624.77
	B4	35433.3	97714.7	—	59369.4	25842.3	44597.4	370232.7	56574.2	53.7	228.0	4.6	183560.84
	B5	32660.1	75564.7	56984.3	66768.9	25842.3	44597.4	415612.5	101954.1	112.5	228.0	4.0	384583.51

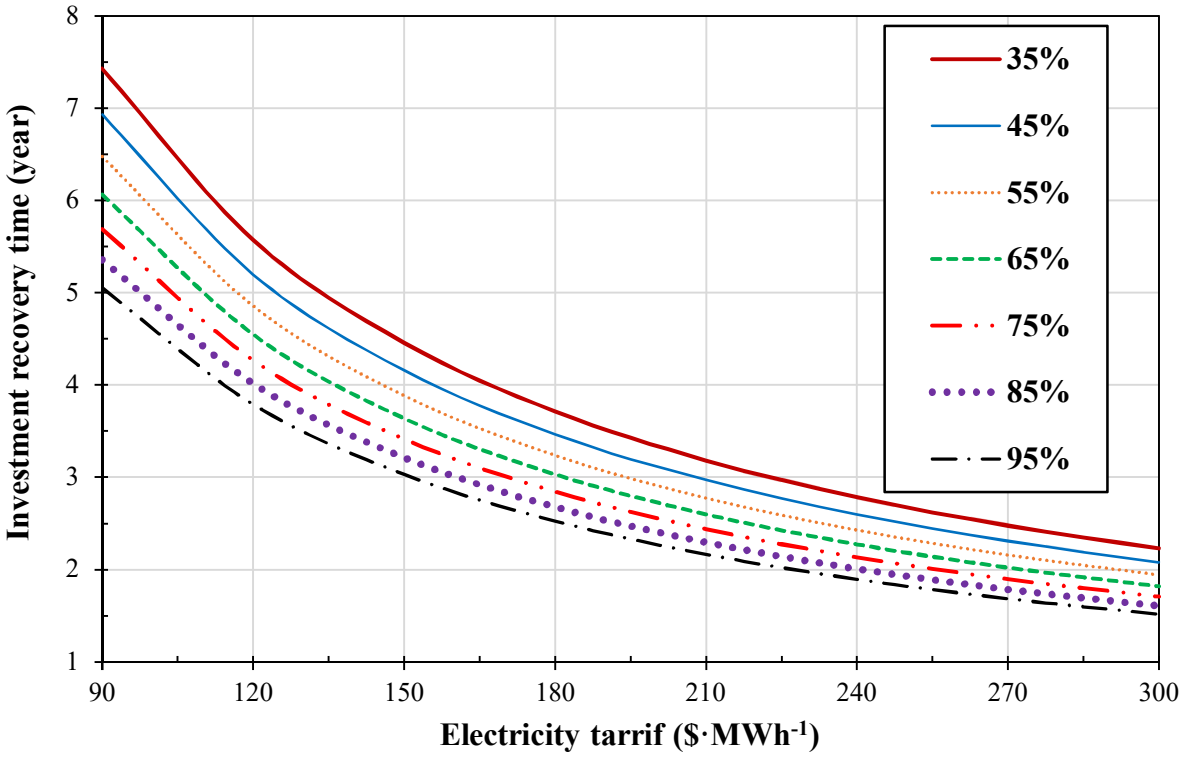

Fig. 6.16 Effect of expander isentropic efficiency and electricity tariff on investment recovery time for B5 operating in climatic conditions of New Delhi

6.1.4 Performance comparison of booster and indirect/cascade configurations

Fig. 6.17 compares the COPs, computed as the ratio of the sum of the total cooling capacity (MT and LT) to the sum of the total required power input (compressors, fans and, if necessary, pumps), at different outdoor temperatures. B2 have the highest COP at ambient temperatures below 15 °C, whereas the indirect configurations, CSC and FCSC, show the worst performance. At higher external temperatures (i.e. above 30 °C), CSC and FCSC performs energetically better as compared to R and B2. FCSC and CSC show similar performance with increase in the external temperature owing to the modest difference in LT.

The annual energy consumption is calculated as the sum of the hourly energy used to run compressors, fans and, if necessary, pumps over the year. The results are summarized in Table 6.5.

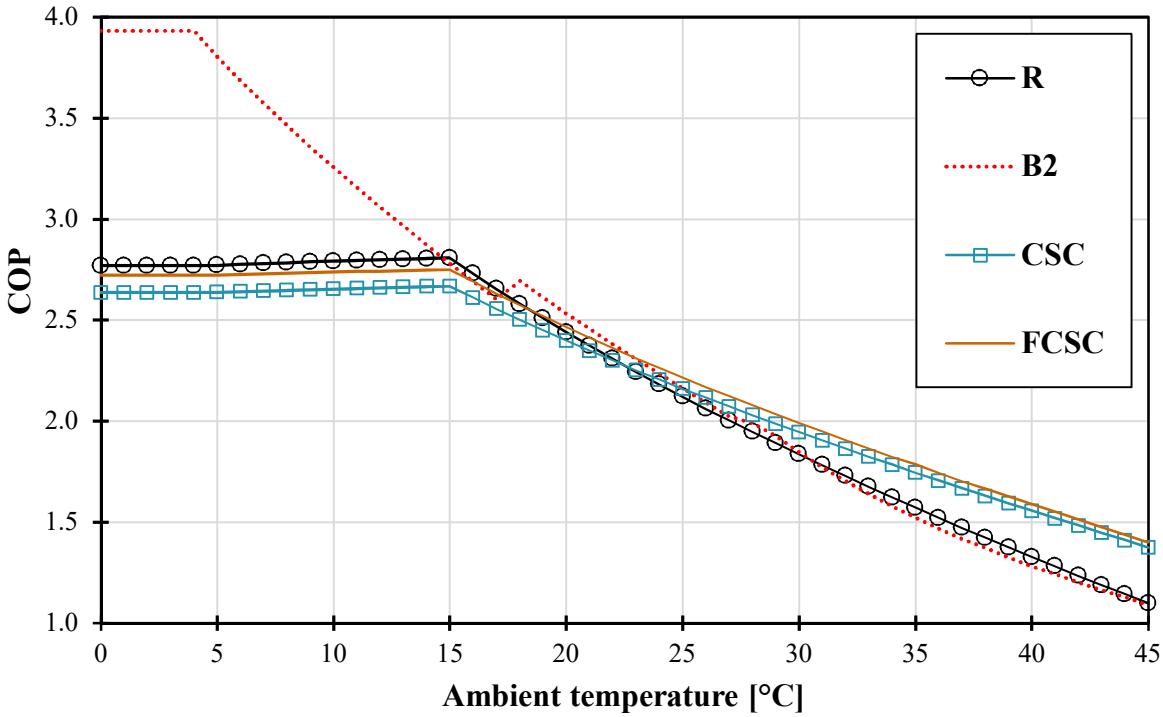

Fig. 6.17 Comparison of COP R, B2, CSC and FCSC configurations

Table 6.5 Annual energy consumption (MWh) of B2, CSC, FCSC and R configurations

System	Seville	Teheran	Phoenix	New Delhi
R	459.6	470.6	552.1	591.1
B2	440.0	439.5	541.1	586.3
CSC	461.6	467.7	532.9	567.2
FCSC	449.1	455.2	519.5	553.4

Being Seville characterized by the least hot climatic conditions among the evaluated locations, B2 represent the best replacement to R in this place with an energy saving by 4.3%. Although Teheran reaches high outdoor temperatures over the year, the B2 configurations can annually operate in sub-critical conditions for many hours, allowing them to consume at least 6.6% less energy than the baseline (R). As for the hottest locations and in comparison, with R, FCSC drop the energy consumption by 5.9% in Phoenix and by 6.4% in New Delhi. In such locations, interesting outcomes can also be associated with CSC as it consumes 3.5% in Phoenix and 4% in New Delhi less energy than R.

6.2 Integrated configurations

As reported in literature, the integrated CO_2 booster system with multi-jet ejector are exciting development and is claimed to be effective in warm climate of Europe. It is also commercially tested in various supermarket located in Northern part of Europe. Danfoss holds the patent of multi-jet ejector. However, it is important to note that the frequency of ambient temperature over shooting 25°C in Europe (for example, Seville) is only 20% (Fig. 6.18). Climate condition in most part of India and Middle East are more extreme. The ambient temperature in Jodhpur, India and in Kuwait, Middle East crosses 25°C for more than 50%. Further in such condition, the A/C load are comparable to the refrigeration load.

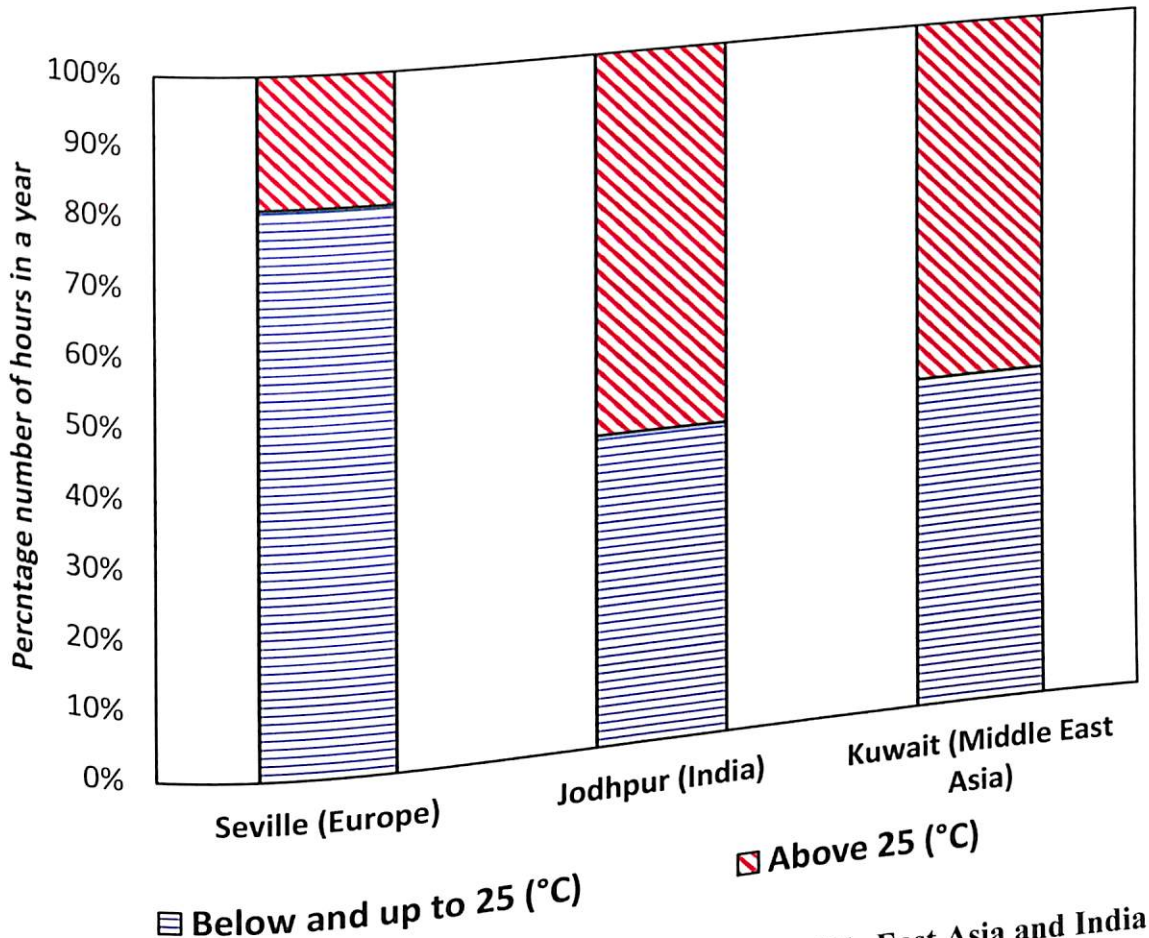

Fig. 6.18 Comparison of warm climate in Europe with Middle East Asia and India

Consequently, this section proposes an all-natural integrated NH_3/CO_2 cascaded booster system for operation in cities with extreme weather conditions like Jodhpur in India

and Kuwait in Middle East. The performance is compared with that of an integrated all-CO_2 multi ejector system and a conventional R404A direct expansion (DX) system without integration.

For conventional R404A DX refrigeration system (abbreviated as 'R'), a separate R410A DX system is chosen to satisfy the A/C load and a R407C DX system to the satisfy heating loads. The comparitive study of integrated configurations is conducted based on both energy and Life Cycle Climate Performance (LCCP) perspectives.

6.2.1 Multi-jet ejector configuration

An integrated "all CO_2" configuration with flooded medium temperature (MT) evaporator, parallel compressor and multi-ejector unit is shown in Fig. 6.19. This configuration is abbreviated as *'B'*. The multi ejector unit consists of a combination of vapor and liquid ejectors (Hafner et al., 2014). Typically, 4 to 6 vapor ejectors and 2 to 3 liquid ejectors each with fixed geometry but different sizes are connected in parallel to constitute multi-jet ejector module. The vapor ejector ensures the occurrence of optimal gas cooler pressure corresponding to ambient conditions as well as entrain a portion of refrigerant from the medium pressure (MP) receiver and compresses the same to the higher IP receiver pressure. Consequently, there is reduction in required high stage (HS) compressors capacity and power consumption. The liquid ejectors pump liquid back to the IP receiver to ensure overfeeding of the MT evaporators. A parallel compressor is adopted to remove the flash gas from the liquid receiver (IP). These compressors are supposed to be switched off in sub-critical operating mode, and the flash gas from the receiver IP is throttled to the MP via a bypass valve, owing to insufficient volume flow rate of the flash gas. An additional A/C heat exchanger is installed to meet the A/C load, while a de-superheater reclaims the required heating demands following a strategy discussed later in section 6.2.4.

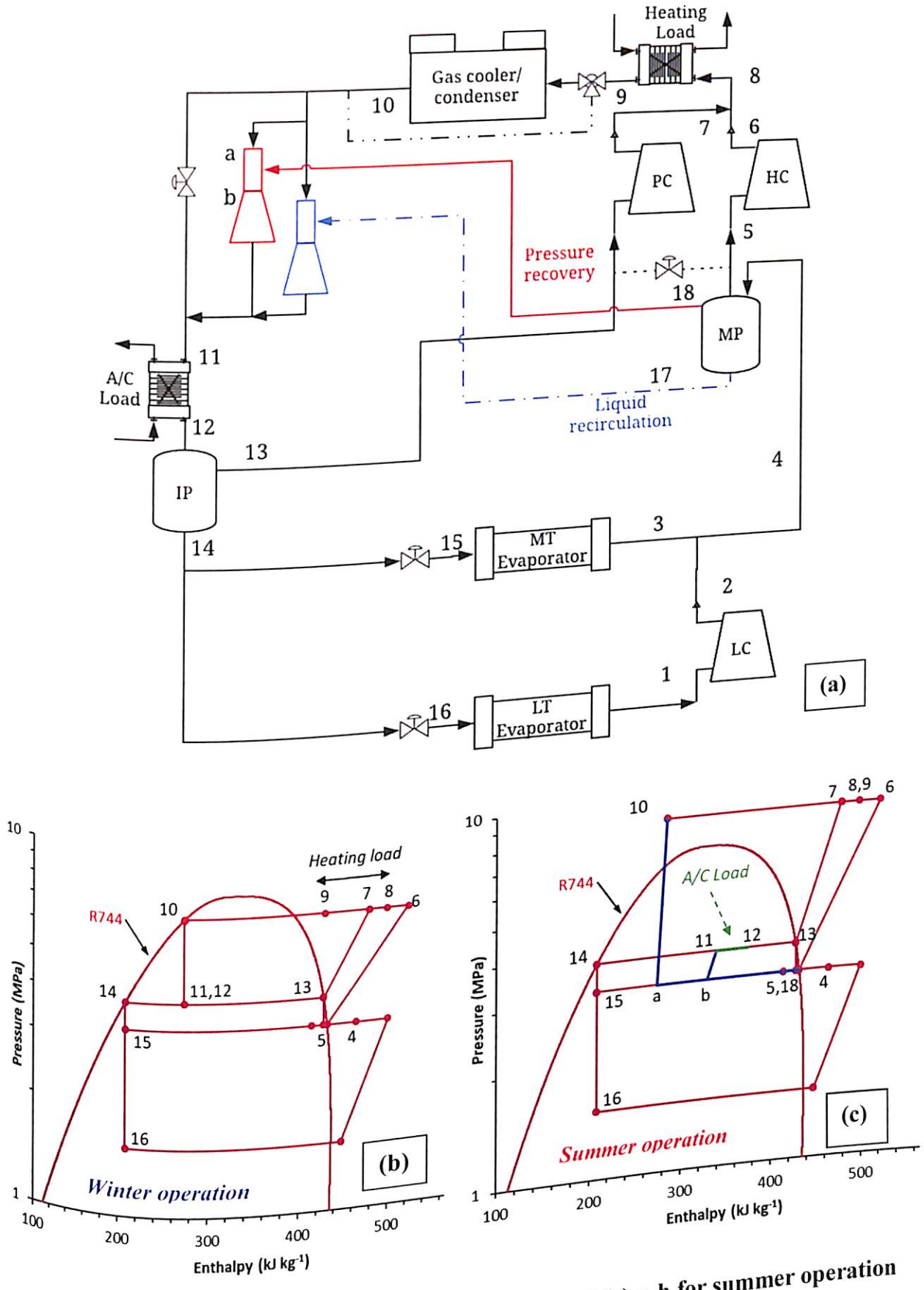

Fig. 6.19 (a) Schematic, (b) p-h for winter operation and (c) p-h for summer operation of an integrated all CO_2 booster system with multi-ejectors

6.2.2 Cascaded booster configuration

The proposed integrated 'all-natural' NH_3/CO_2 cascaded booster configuration, shown in Fig. 6.20, is abbreviated as *'CB'* in this article. The CB configuration is composed of a CO_2 booster system in the low-temperature circuit to cater refrigeration (LT and MT) as well as A/C and heating demands, while ammonia in the high-temperature circuit facilitates efficient heat. At lower ambient (below 18°C), the CB configuration operates as booster configuration. While at high ambient (above 18°C), the CB configuration runs in cascade mode. CB configuration also has a parallel compressor installed in CO_2 side to support the A/C evaporator.

Ammonia refrigeration system are known to be most common and efficienct technology in industrial installations. However, owing to the reduced charge and improved component efficiency, nowadays these systems are also considered as viable alternatives in commercial sector, especially for the warm climate operation (Pearson, 2008). Ammonia units is proposed to be isolated by installing the same in machine room in a supermarket with neccesary safety measures. Hydrous ammonia is known to be corrosive to copper, zinc and copper-alloys, while the standard material used in ammonia system is structural steel and aluminium. Typical equipment required for safe handling of ammonia include, ammonia leak detector having visual and audio alarm, spark proof emergency ventilating system, ammonia scrubber, self-closing doors, fire extinguishers, protective goggles, gloves, protective clothing, emergency eye-wash fountain (Stene, 2008) etc.

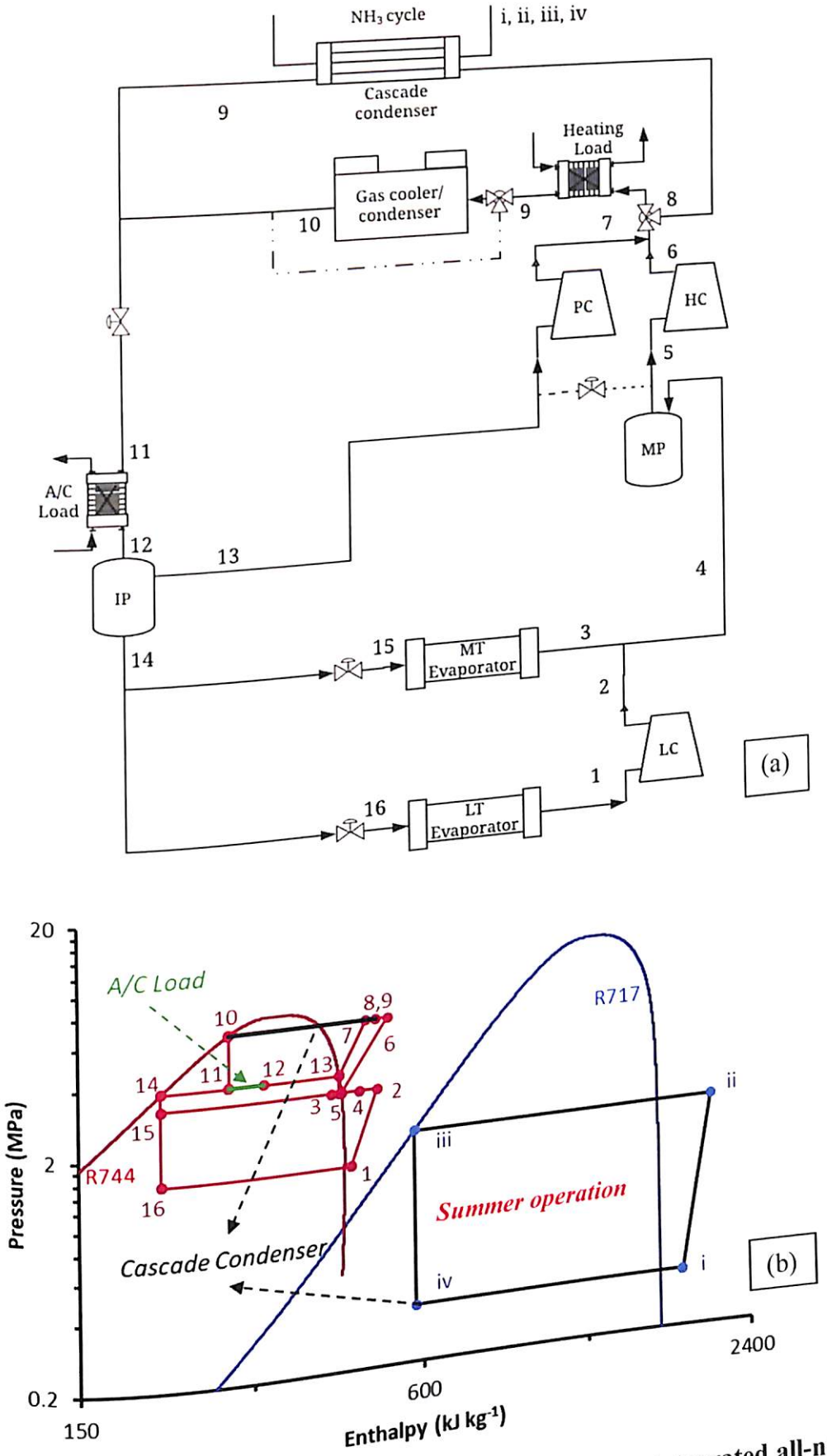

Fig. 6.20 (a) Schematic and (b) p-h for summer operation of an integrated all-natural NH_3/CO_2 cascaded booster system

6.2.3 Load computation

EnergyPlus (Deru et al., 2011) is used to formulate the refrigeration, A/C and heating loads in the climate regions of the Middle East and India. A standard supermarket with a floor area of approximately 3,590 m^2 is assumed, which is divided into four zones vestibule, deli, sales, and backroom. The LT, MT and A/C evaporation temperature levels assumed, are -35°C, -10°C and 5°C, respectively. The model is developed based on detailed weather and building construction data, including internal loads consisting of lighting, average foot fall, electric and gas loads. The exterior wall construction for the conceptual design consists, from the exterior to the interior stucco, a concrete block, a layer of insulation, and gypsum board. The details of the supermarket configuration and A/C as well as heating load calculated from the model on monthly basis are listed in Table 6.6. For the article, Beta (β) is defined as the averaged A/C load to the total averaged refrigeration load while Lambda (λ) is the ratio of averaged heating load to the total averaged refrigeration load. The discussion on the typical climatic conditions and refrigeration as well as A/C and heating loads prevailing in Middle East Asia and India are presented in the following subsections.

Middle East Asia has two major climatic zones, Midlatitude represented by Tabriz and Damascus, and Dry Arid/Semi-Arid, as in Tehran, Cairo, Kuwait and Abu Dhabi. As reported in the literature (Karampour and Sawalha, 2018), LT load is nearly constant for all the locations, while MT load, as well as A/C and heating loads are dependent primarily on the ambient temperature and secondly on the relative humidity (Fig. 6.21 (a)). With increase in average ambient temperature, the MT load and A/C load are found to rise. On the contrary, the heating load is found to increase with a decrease in ambient. The average ambient temperature in winter (January) is recorded to be minimum of -2.65°C in Tabriz in lower side and 18.15°C in Kuwait in higher side. For summers (June), the maximum averaged outside air temperature is 21.55°C in Tabriz in the lower side and 36.9°C in Kuwait in higher side.

Yearly averaged ambient temperature is 12.15°C in Tabriz and 26.63°C in Kuwait. Being a relatively cold place, Tabriz has the highest heating load of 158.67 (kW) and minimum A/C load of 28.40 (kW). While Kuwait have high A/C load of 119.26 (kW) and comparably low heating load of 43.36 (kW). Fig. 6.21 (b) compares the climatic conditions in a few cities in Middle East to that in Europe. Referring to Fig. 6.21 (b), λ in Tabriz goes up to 1.3, which is well above the maximum value reported in Europe. While the β is significantly higher and goes up to 0.87 for Kuwait.

Table 6.6 Supermarket configuration and monthly averaged heating & A/C load

SUPERMARKET CONFIGURATION	
Floor Area (m^2)	3590
Height (m)	3
Wall Thickness (Stucco/Concrete Block/Insulation/Gypsum Board) (m)	0.025/0.203/0.175/0.0127
Thermal Conductivity of wall (Stucco/Concrete Block/Insulation/Gypsum Board) ($W \cdot m^{-1} \cdot K^{-1}$)	0.691/1.31/0.049/0.160
Density of wall (Stucco/Concrete Block/Insulation/Gypsum Board) ($kg \cdot m^{-3}$)	1858/2240/265/785
Specific Heat of Wall (Stucco/Concrete Block/Insulation/Gypsum Board) ($J \cdot kg^{-1} \cdot K^{-1}$)	837/836.8/836.8/830
Thermal Transmittance of wall ($W \cdot m^{-2} \cdot K^{-1}$)	0.26
Void to Solid Ratio (Ratio between opaque and transparent surfaces)	0.30
Thermal/Solar/Visible Absorptance of Stucco (-)	0.90/0.92/0.92
Thermal/Solar/Visible Absorptance of Concrete Block (-)	0.90/0.70/0.70
Thermal/Solar/Visible Absorptance of Insulation (-)	0.90/0.70/0.70
Thermal/Solar/Visible Absorptance of Gypsum Board (-)	0.90/0.92/0.92
MONTHLY AVERGAED HEATING & A/C LOADS	
Avg. Heating Load in January* (Tabriz, Middle East) (kW)	158.67
Avg. Heating Load in January (Shillong, India) (kW)	83.85
Avg. Lambda in January (Tabriz, Middle East) (-)	1.3
Avg. Lambda in January (Shillong, India) (-)	0.63
Avg. A/C Load in June# (Kuwait, Middle East) (kW)	119.26
Avg. A/C Load in June (Jodhpur, India) (kW)	137.80
Avg. Beta in June (Kuwait, Middle East) (-)	0.87
Avg. Beta in June (Jodhpur, India) (-)	0.94

* Coldest month, # Hottest month

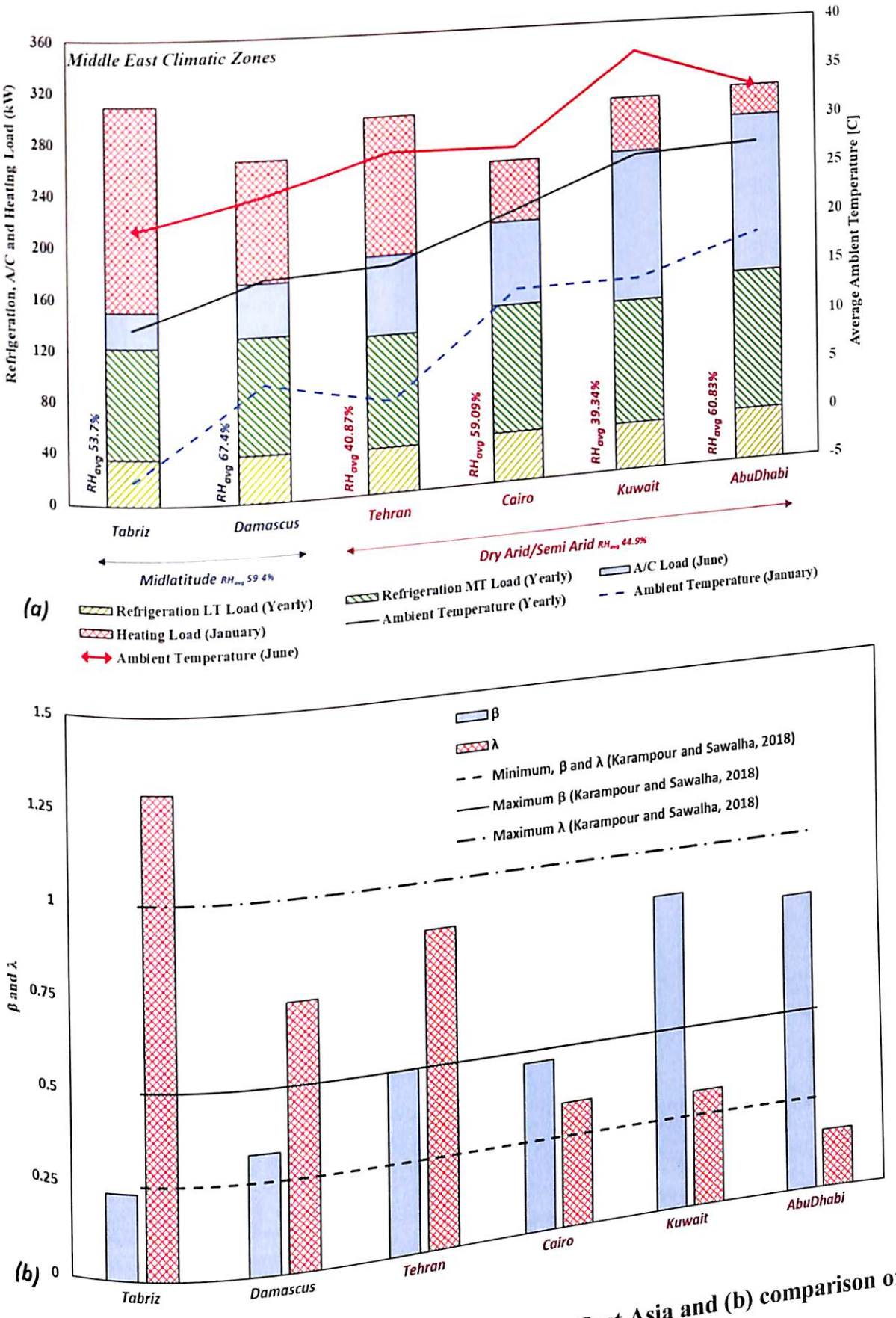

Fig. 6.21 Year-round climate conditions of (a) Middle East Asia and (b) comparison of typical heating and A/C load to that of European climate

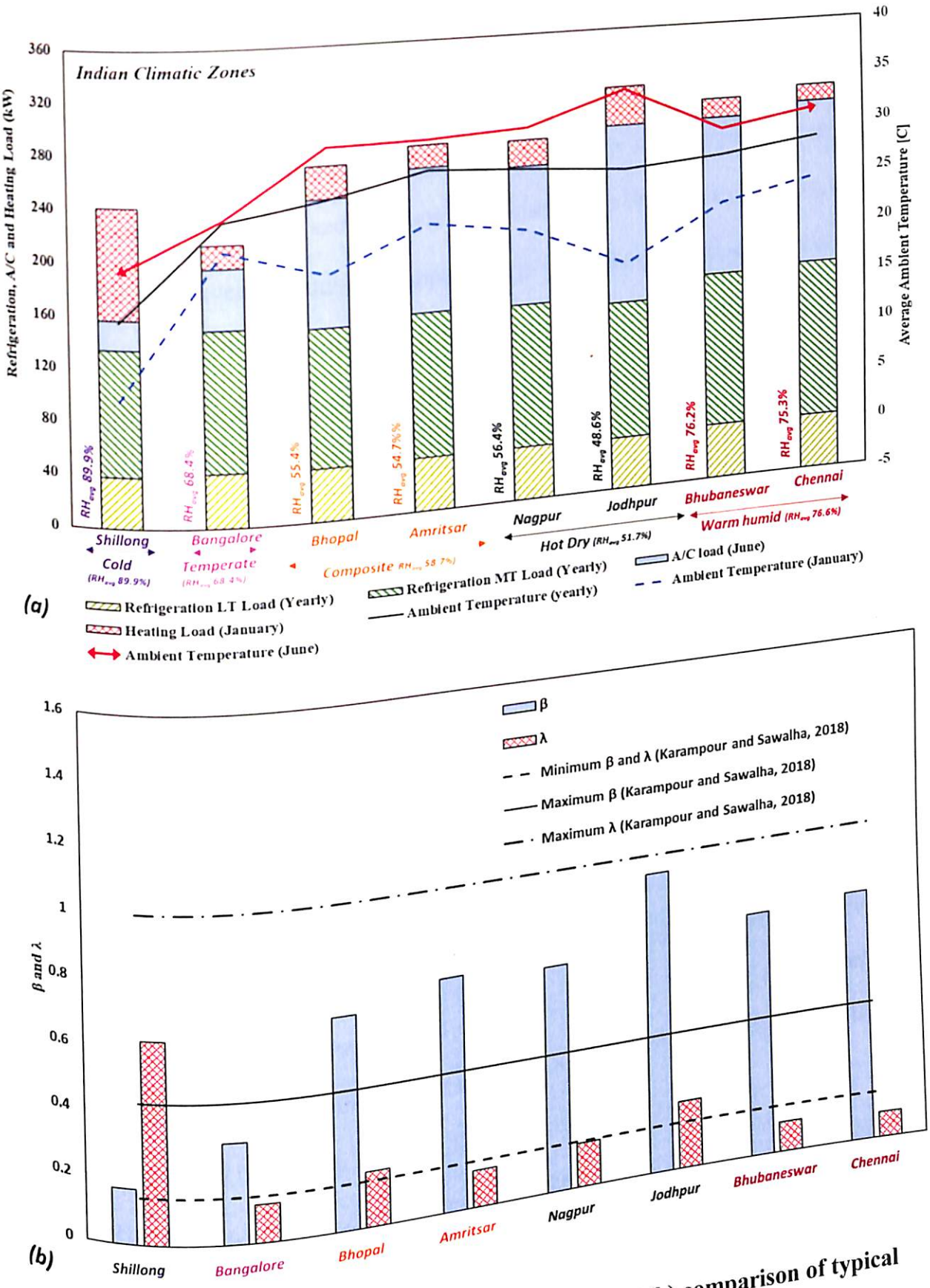

Fig. 6.22 Year-round climate conditions of (a) India and (b) comparison of typical heating and A/C load to that of European climate

There are five climatic zones in India which include Cold (Shillong), Temperate (Bangalore), Composite (Bhopal and Amritsar), Hot Dry (Nagpur and Jodhpur) and Warm Humid (Bhubaneswar and Chennai). The climatic zones in a set of representative cities in India are shown in Fig 6.22 (a) and the same is compared with that in Europe in Fig. 6.22 (b). The maximum daily averaged ambient temperature in summers (June) is recorded of 19.12°C for Shillong and 34.03°C for Jodhpur. For winters, the daily averaged minimum outside air temperature is 6.93°C in Shillong, and the same goes maximum to 17.01°C in Jodhpur. Yearly averaged ambient temperature is 19.12°C in Shillong, while 28.33°C, 27.03°C and 26.20°C in Chennai, Bhubaneshwar and Jodhpur, respectively. The reason for such high yearly average ambient temperature in Chennai and Bhubaneswar (both in coastal region), is due to the comparatively higher relative humidity (see, Fig 6.22 (a)). Shillong has the highest heating load of 83.85 (kW) and minimum A/C load of 22.80 (kW). Being warm locations, Jodhpur (Hot Dry) and Chennai (Warm Humid) have the maximum A/C load, of 137.80 (kW) and 128.74 (kW), respectively. Heating loads for Jodhpur and Chennai are 30.23 (kW) and 12.41 (kW), respectively. Bangalore has lower A/C loads as well as lower heating load. Bhopal (Composite) and Jodhpur (Hot Dry) also has similar climatic conditions, except that Jodhpur has higher A/C load as well as heating load, owing to comparatively higher and lower average temperature in summer and winter, respectively. Fig. 6.22 (b) compares the climatic conditions in India to that in Europe. As observable from the Fig. 6.22 (b), λ in Shillong is just above 0.6, which is below the maximum value reported in Europe. For Hot Dry/Warm Humid locations and in comparison, with Europe, the β in Chennai and Jodhpur is significantly higher and goes maximum up to 0.78 and 0.94.

6.2.4 *Model and load integration*

Mass and energy balance across each components of the cycles are applied assuming steady-state operation, no heat transfer and no pressure loss in piping and isenthalpic expansion in

the expansion valve. The minimum condensing temperature for CO_2 is 7°C, while the same is 25°C for the NH_3 condensers. In CB configuration, the condensing temperature of CO_2 is 10°C, while the NH_3 rejects the heat outdoor. Approach temperature of 10°C is considered for all condenser, except for CO_2 gas cooler/condenser, which are adopted from those reported in Gullo et al., (2017). Approach temperature for cascade condenser in CB system is 5°C.

In the overfed evaporator, the refrigerant enters with a low vapor quality and leaves in two-phase with high vapor quality, owing to the excess liquid circulation for such heat exchangers. As a result, more liquid is transferring heat, allowing the saturation temperature of overfed evaporators to be higher than that of conventional dry evaporators. Consequently, for MT overfed evaporator, an increase of 6 K in saturation temperature is adopted (Wiedenmann, 2015). The internal superheat as well as external superheat of 5°C each, are assumed for all the dry evaporators. While a vapor quality of 0.9 is assumed at the exit of MT overfed evaporator in B configuration. The air-cooled gas cooler/condenser fan power for both B and CB systems is assumed 3% of the gas cooler/condenser heat duty (Karampour and Sawalha, 2018).

The operating conditions of ejector viz entrainment ratio defined as ratio of mass flow rate associated with suction flow to the mass flow rate at the motive flow, operating gas cooler pressure, receiver pressure (generally fixed) and ambient conditions significantly affects the ejector efficiency as well as the overall system performance. Of course, geometry of ejector itself plays a vital role in predicting the on-design as well as the off-design performance of ejector. Consequently, multi-jet ejector module in this article is modelled following the methodology adopted by Gullo et al., (2017). The methodology suggested by Gullo et al., (2017) is utilizes experimental data in literature to formulate correlations to predict entrainment ratio in terms of pressure lift (difference between pressure of receiver IP

and MP) and the gas cooler/condenser outlet temperature. The minimum and maximum values for the pressure lift, adopted from the literature, are 4 bar and 15 bar, respectively. The upper limit of ejector efficiency is kept 0.40 (Elbel and Hrnjak, 2008). The ejector module is modelled by optimizing the pressure lift for the varying ambient conditions.

At ambient temperature lower than 18°C, both B and CB configurations operate similarly, as the ammonia chiller is not operational below 18°C. The consolidated operating parameters are listed in Table 6.7.

Table 6.7 Operating parameters of the investigated integrated systems

Parameter	*Assumed value*
Minimum condensing temperature of CO_2/NH_3	7°C/25°C
Minimum condensing temperature of DX R404A	25°C
Approach temperature for NH_3 condenser	10°C
Approach temperature for DX R404A condenser	10°C
CO_2 gas cooler/condenser outlet temperature	T_{amb}+3°C (4°C<T_{amb}<=17°C) (0.9×T_{amb})+4.7°C (17°C<T_{amb}<=27°C) T_{amb}+2°C (T_{amb}>27°C)
Approach temperature for cascade condenser	5°C
Internal/External superheating (Dry evaporator)	5°C/5°C
Vapor quality at outlet of flooded evaporator	0.9
Air cooled gas cooler/condenser fan power	3% of the gas cooler/condenser load
Compressor efficiencies	calculated as a function of pressure ratio using manufacture data

A/C evaporator is switched on above 17°C ambient temperature. Otherwise, ambient cooling is assumed effective. CO_2 receiver and parallel compressor are designed to satisfy the

A/C load for both B and CB configurations. The supply and return temperature for A/C load is taken as 7°C and 12°C, respectively, (ARI, 2003).

Heat recovery mode becomes active in both B and CB configurations when the ambient temperature is less than 18°C. The supply temperature for heating loads is considered as 35°C and 45°C at the ambient temperature above and below 0°C, respectively (Karampour and Sawalha, 2018). Any further heating demand is met using auxiliary heaters with assumed conversion efficiency of 0.95.

A de-superheater installed (see, Fig. 6.19) reclaims the superheat of the CO_2 following the control strategy suggested by Sawalha (2013). Normally, the gas cooler is operated at full capacity for minimum possible gas cooler exit temperature, regulating the high side pressure to meet the required heating load in the integrated system. The increment in high side pressure to meet the heating load is limited to an optimum value corresponding to the system maximum efficiency. To meet the required heating load beyond the maximum operating pressure limit, as a second step, the gas cooler capacity is reduced to increase the CO_2 temperature at the exit of the gas cooler.

6.2.5 *Standalone heat pump and A/C system*

A standalone heat pump is modelled as an air source heat pump (SHP), with R407C as operating fluid. As per Karampour and Sawalha, (2018) following data are assumed: total superheat of 10°C, defrost energy consumption equals 7% of compressor power, minimum evaporator temperature of -15°C and evaporator approach temperature of 7.5°C. For very-low ambient temperature, auxiliary heaters are installed to support the SS to meet the heating load. For space cooling, standalone HFC based A/C, using R410A, is modelled considering evaporation temperature of 3°C, total superheat of 10°C and condenser approach temperature of 10°C. Both the standalone A/C and heat pump are modelled assuming compressor isentropic efficiency of 0.70.

6.2.6 Energy and Life Cycle Climate Performance (LCCP) analysis

The combined COP, termed as COP_{total} is defined as the ratio of total load including refrigeration as well as A/C and heating load to the total power consumption expressed as equation (6.9).

$$COP_{total} = \frac{\dot{Q}_{LT} + \dot{Q}_{MT} + \dot{Q}_{A/C} + \dot{Q}_{H}}{\dot{W}_{total}} \tag{6.9}$$

The parallel compressors are assumed to be large enough to compress all vapor generated owing to the integration of A/C load. COP of A/C integration in the B configuration is calculated as the ratio of A/C load to increase in power consumption for the parallel compressor. While, in CB configuration, COP of A/C integration is calculated as the ratio of A/C load to increase in power consumption for both parallel CO_2 compressor and NH_3 compressor.

To calculate the heating COP for both B and CB configurations, the power required for the heating system is calculated as difference in total power consumed while operating with heating load and power consumed while satisfying only the refrigeration load (Karampour and Sawalha, 2018). Fig. 6.23 and Fig. 6.24 represents the flow chart for simulation of B and CB configuration, respectively.

LCCP is a very effective tool to assess the environmental impact of a refrigeration system (Beshr et al. 2015). The parameters include lifetime energy efficiency, the specific refrigerant in use and the lifetime refrigerant emissions. LCCP, expressed as in equation (6.10), represents the total CO_2 equivalent emissions for a refrigeration system including both direct and indirect emissions. The direct emissions, expressed as in equation (6.11), include emissions related to leakage/escape of refrigerant from the system, refrigerant loss at the end of life of the system and refrigerant loss during service events (Beshr et al., 2015). The indirect emissions, given by equation (6.12), include emissions related to production and

distribution of electric energy consumed by the refrigeration system as well as emissions related to manufacturing the machinery and the recycling of the machinery at the end of life. The various parameters assumed to calculate LCCP are consolidated in Table 6.8.

$$LCCP = Em_{direct} + Em_{indirect} \quad (6.10)$$

$$Em_{direct} = Em_{leakage} + Em_{EOL} + Em_{service} \quad (6.11)$$

$$Em_{indirect} = Em_{energy} + Em_{manufacture} + Em_{recycle} \quad (6.12)$$

Table 6.8 LCCP analysis assumptions

Parameter	*Assumed value*	*Reference/source*
Refrigerant charge (kg/kW)	CO_2: MT=3, LT=2 Cascade high stage: 0.75 DX/HFC: MT=2, LT=4	(Karampour and Sawalha, 2018)
Leakage rate (%)	10	Percentage of refrigerant leakage to atmosphere
System lifetime (years)	20	(Beshr et al., 2015)
Service interval (years)	2	
Service leak rate (%)	5	
Reused refrigerant (%)	85	
GWP	CO_2 = 1, NH_3 = 0 R404A = 3922 R407C = 1624 R410A= 1924	(ASHRAE, 2014)

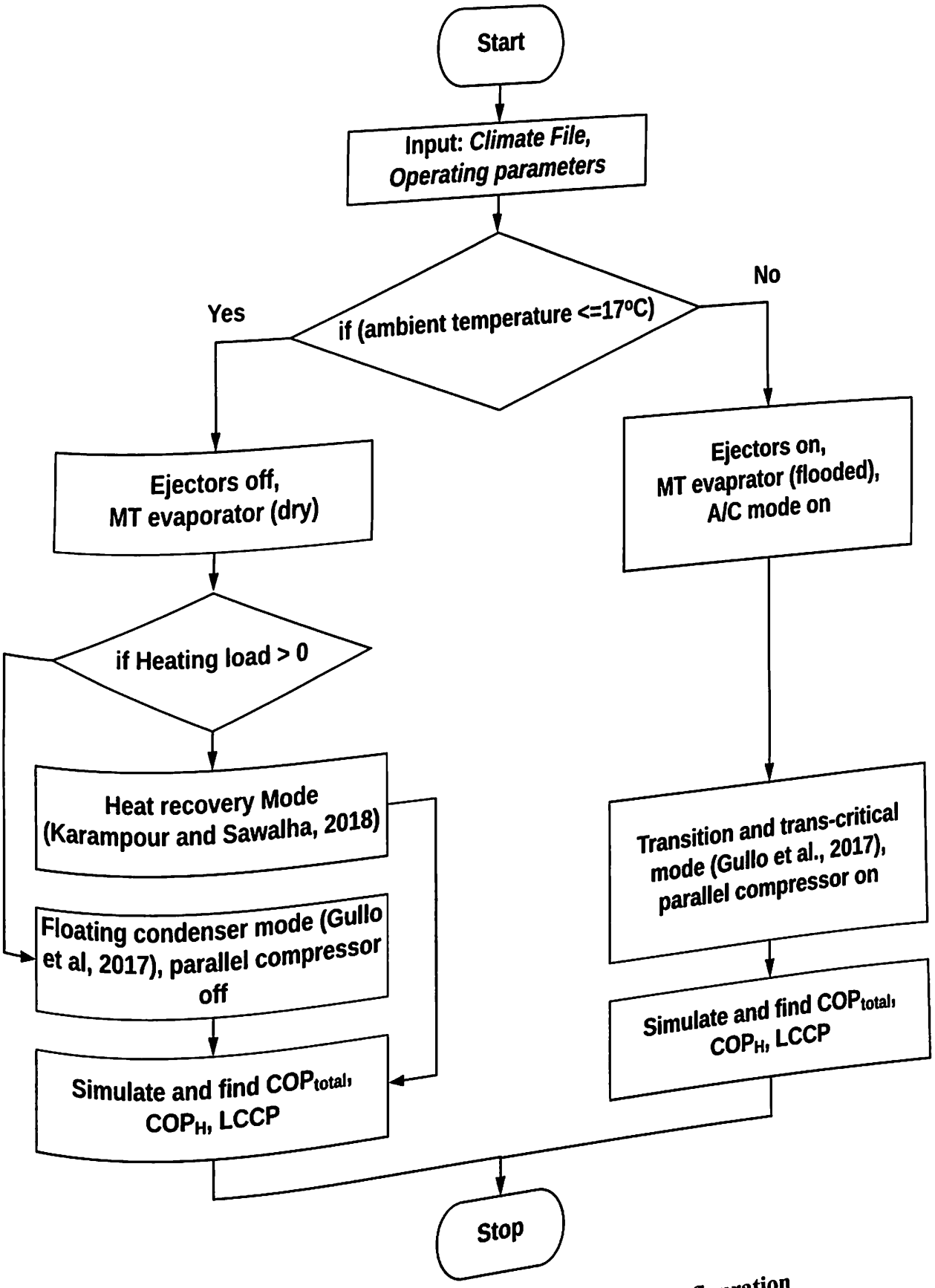

Fig. 6.23 Flowchart for simulation of integrated B configuration

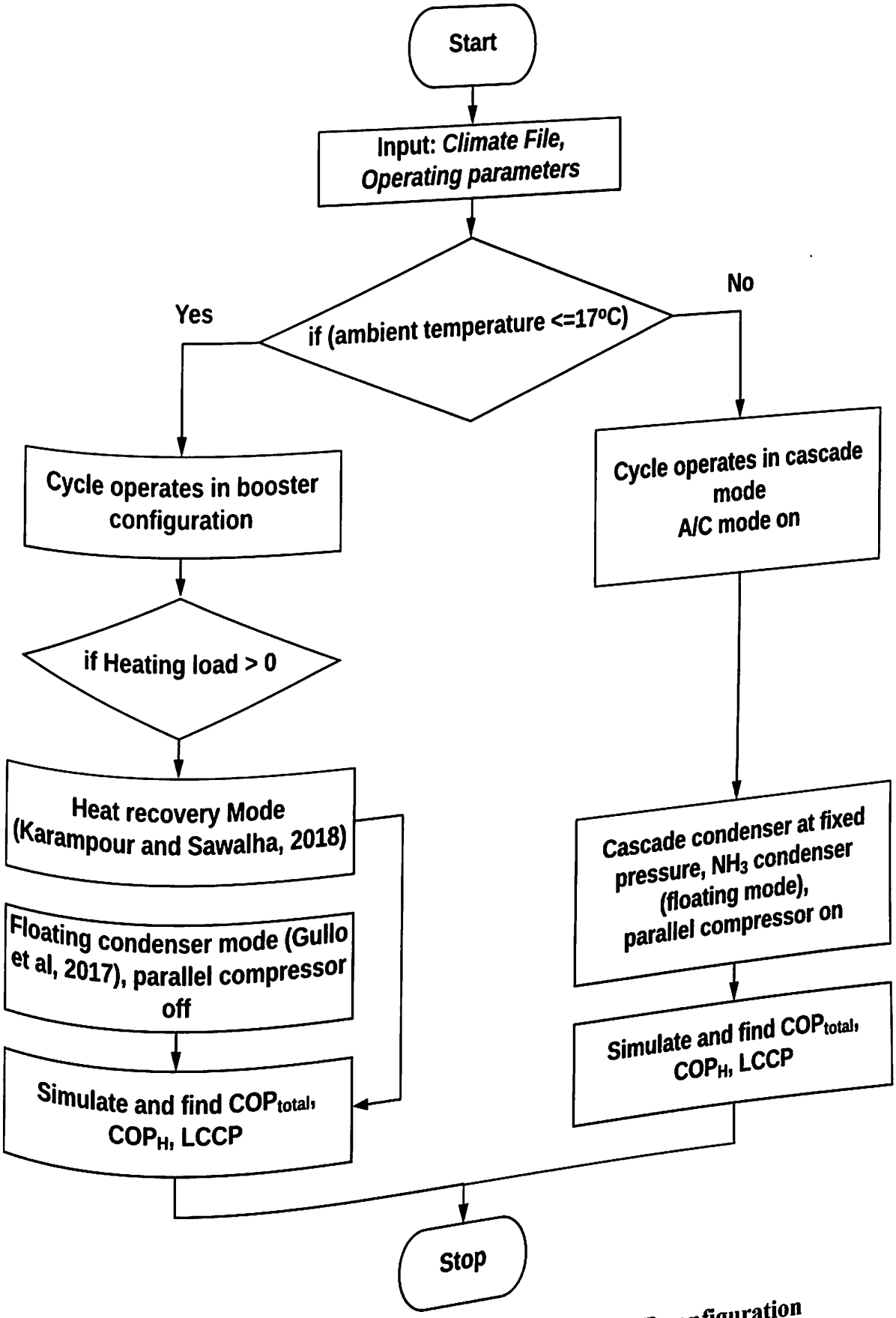

Fig. 6.24 Flowchart for simulation of integrated CB configuration

Fig. 6.25 presents simulated values of COP_{total} for R, B and CB configurations for two cities in Middle East representative, of the two climate zones, while Fig. 6.26 and Fig. 6.27 depicts the same for four cities in India, representative of four climate zones. Fig. 6.25 to Fig. 6.27 are plotted for an hourly averaged profile of temperature, refrigeration load as well as A/C and heating load for 24 hours each for both cold and warm months. On the primary axis, COP_{total}, as well as β and λ, are plotted, while the secondary axis shows variation of ambient temperature.

Owing to relatively cold climate prevailing in Tabriz (Fig. 6.25a), compared to Kuwait (Fig. 6.25b) it is observable that, the COP_{total} for B configuration followed by CB, are higher than that of R configuration. The annual average COP for R, B and CB configurations, when operated in Tabriz are found to be 3.18, 3.78 and 3.68, respectively. Similarly, operated in Tabriz, the total emissions for R, B and CB configurations are 19.26 ($kTonsCO_{2eq}$), 7.61 ($kTonsCO_{2eq}$) and 7.80 ($kTonsCO_{2eq}$), respectively. On the contrary, while operating in Kuwait having extreme climate, the performance of CB configuration is found better than that of both B and R configurations. The advantage is apparent for operation during peak summer month of June.

There is a decrement in performance of CB during January due to the operational shift in CB system from the booster to the cascade configuration, when ambient is in the range 18°C to 26°C. For ambient above 26°C, the performance of CB configuration is found better. The ambient temperature in Kuwait remains higher than 25°C, for more than 50% in a year and hence the annual COP_{total}, for CB configuration is found much better. The total emissions for CB configuration operating in Kuwait are also found lower by 51.5% and 11.2% compared to R and B configurations, respectively.

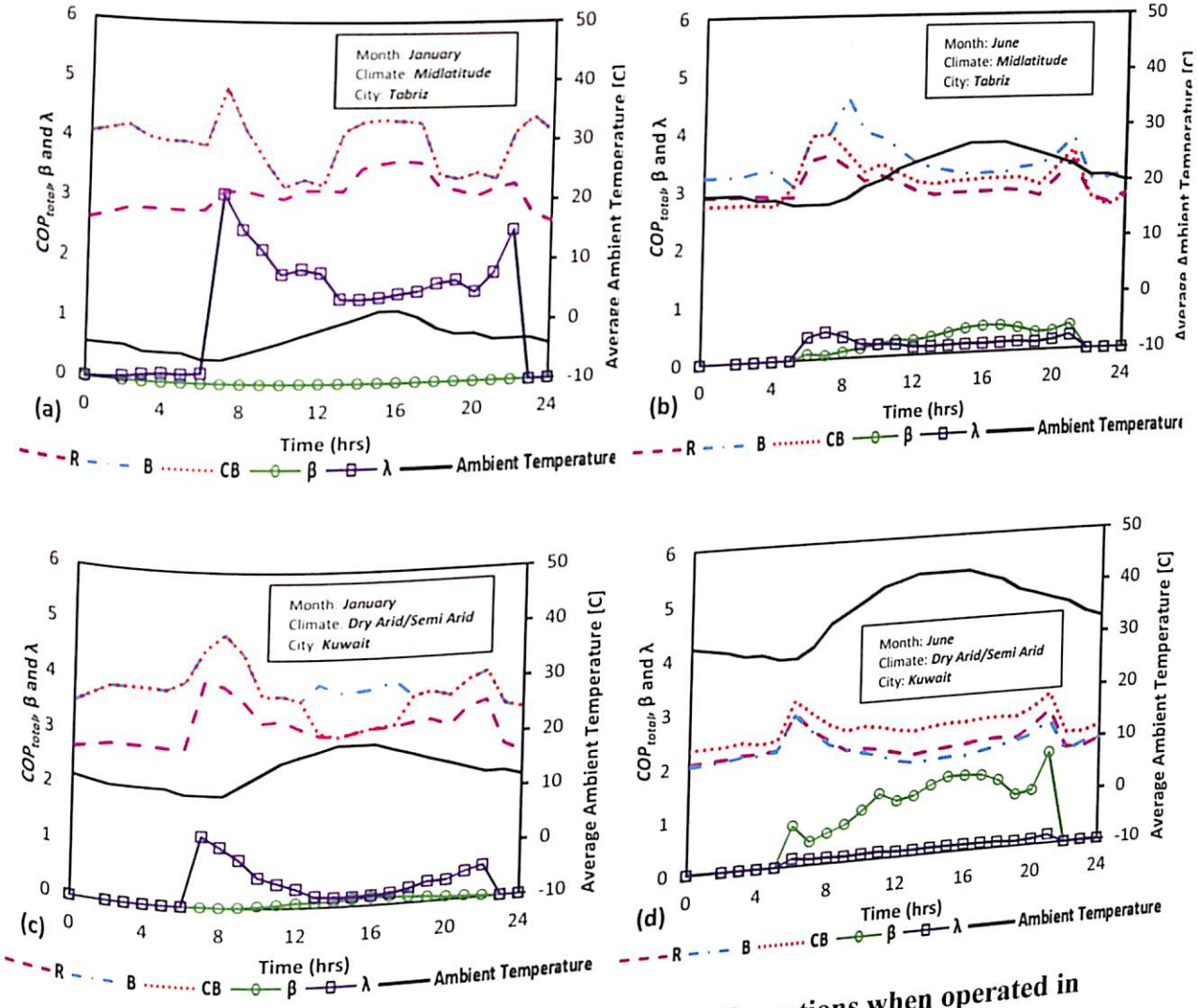

Fig. 6.25 Monthly COP_{total} for R, B and CB configurations when operated in Midlatitude, Tabriz (a & b) and Dry Arid/Semi-Arid, Kuwait (c & d), climates in the Middle East

Fig. 6.26 presents performance of all three investigated systems for operation in Cold (Shillong, subplots a & b) and Temperate (Bangalore, subplots c & d) climates in India. It is observed that configuration B outperforms in both Cold and Temperate climates. The annual COP_{total} for R, B and CB configurations operating in Shillong are found 3.23, 3.90 and 3.62, respectively, while the same are 2.81, 3.09 and 2.96, respectively, for operation in Bangalore. Compared to baseline R configuration, the reduction in total emissions for B and CB configurations for operation in Shillong is found to be 63.7% and 61.1%, respectively, while the same is 54.5% and 52.5% for operation in Bangalore.

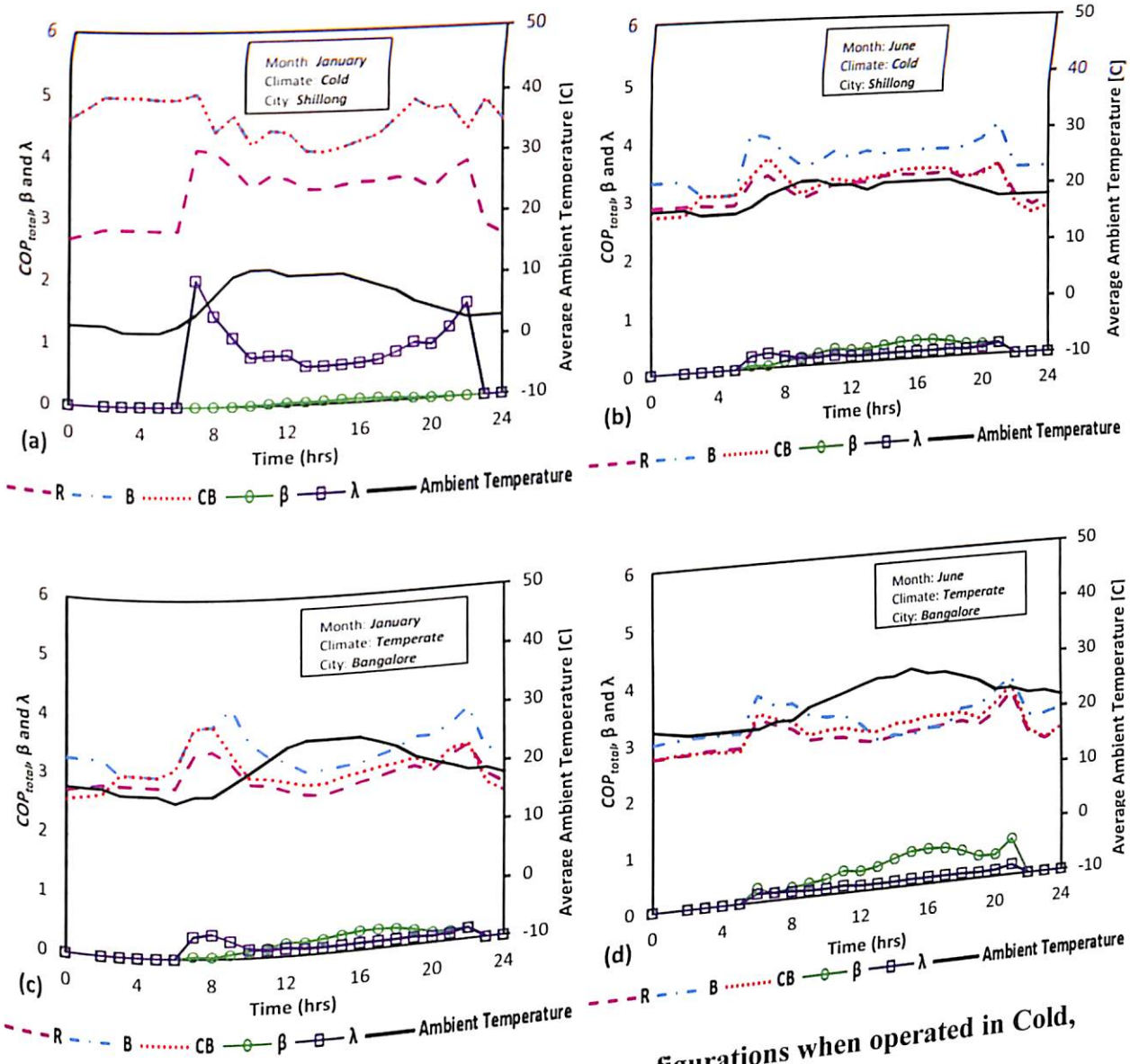

Fig. 6.26 Monthly COP_{total} for R, B and CB configurations when operated in Cold, Shillong (a & b) and Temperate, Bangalore (c & d), climates in India

When simulated for operation in Warm Humid (Chennai) and Hot Dry (Jodhpur) climates in India (Fig. 6.27), it is observed that the CB configuration outperforms both the R and B configurations during the month of June. There is an observable drop in performance for a fraction of duration in the day during the month of January. The same is ascribed to operational shift while the ambient is within range 18°C to 26°C. However, the extended hours of operation of the refrigeration system at ambient above 25°C results in higher

performance of CB configuration by 6.6% and 6.9% compared to B configuration, when operated in Chennai and Jodhpur, respectively.

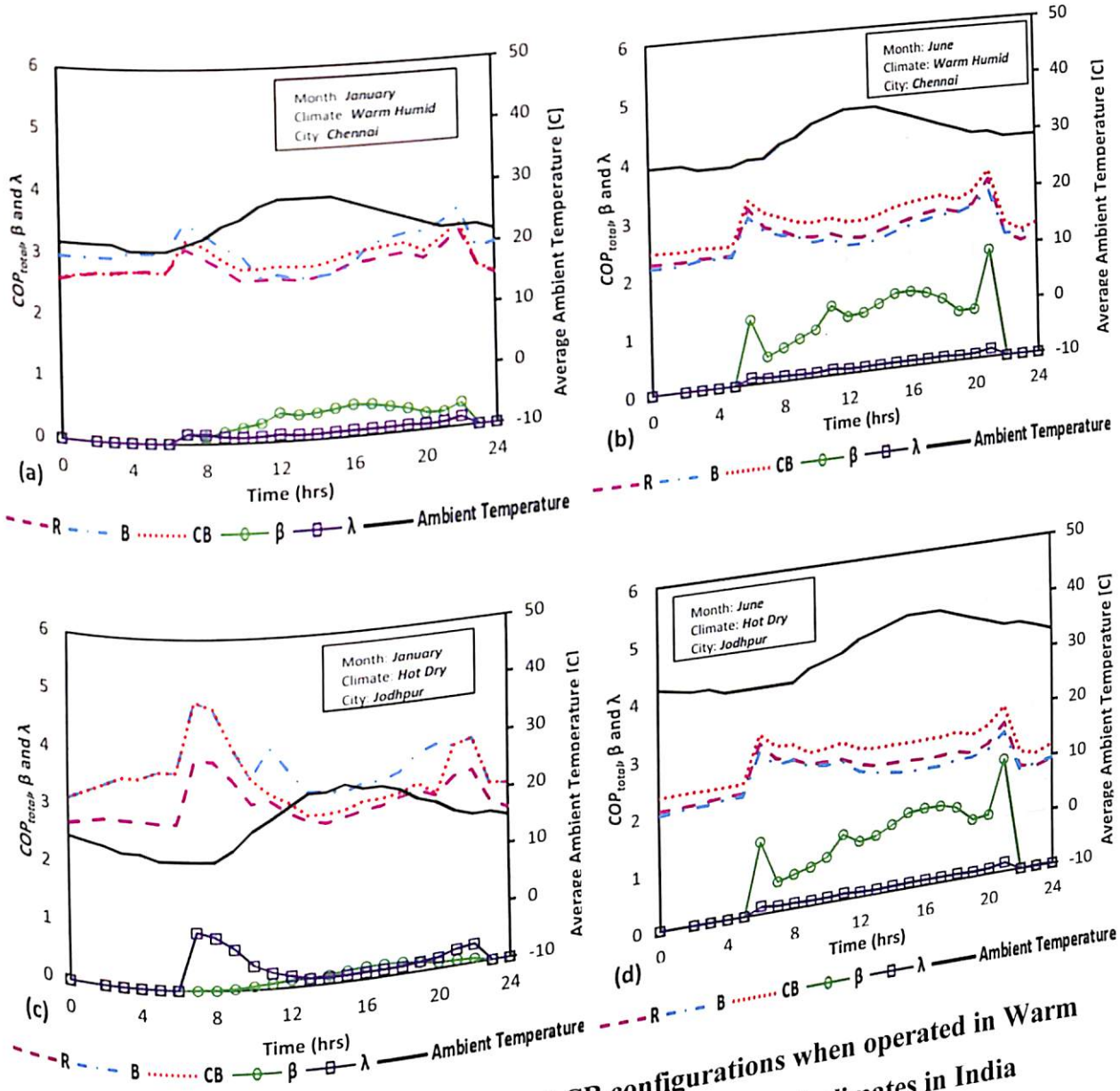

Fig. 6.27 Monthly COP_{total} for R, B and CB configurations when operated in Warm Humid, Chennai (a & b) and Hot Dry, Jodhpur (c & d) climates in India

Fig. 6.28 and Fig. 6.29 compares relative annual COP_{total} and total emissions for R, B and CB configurations, for operation in both Middle East and Indian climatic conditions. Fig. 6.30 compares indirect emissions for all configurations. While Table 6.9 comprehensively presents and compares the absolute values for annual COP_{total} and total emissions for all configurations.

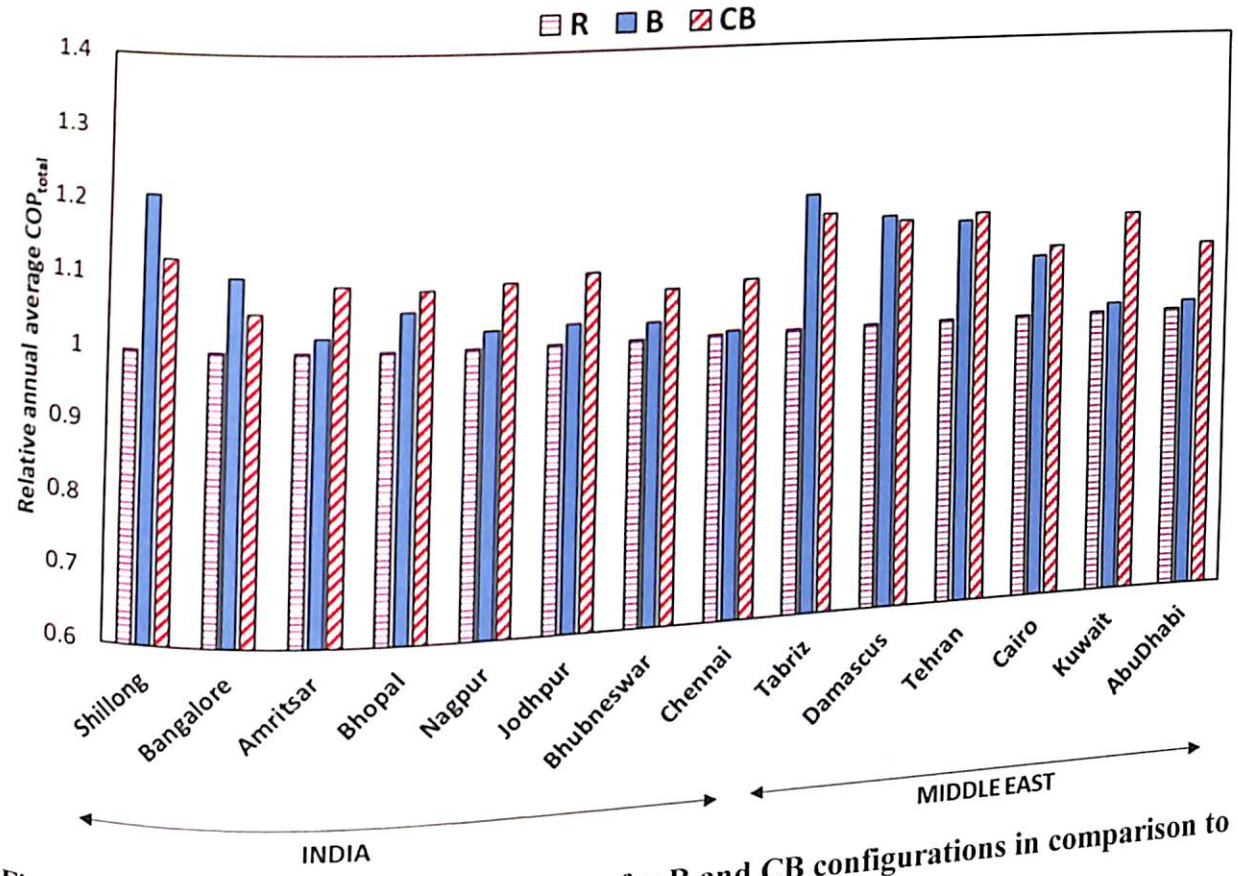

Fig. 6.28 Relative annual average COP_{total} for B and CB configurations in comparison to R configuration

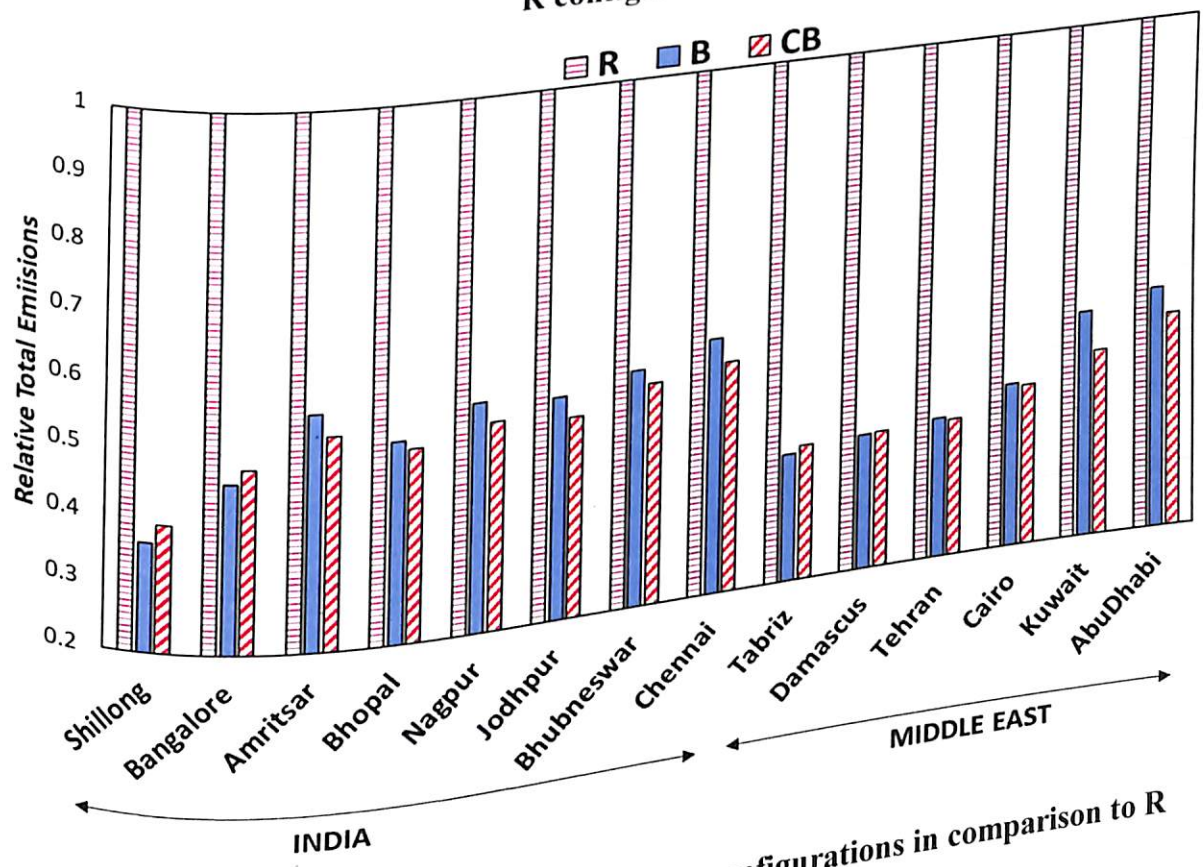

Fig. 6.29 Relative total emissions for B and CB configurations in comparison to R configuration

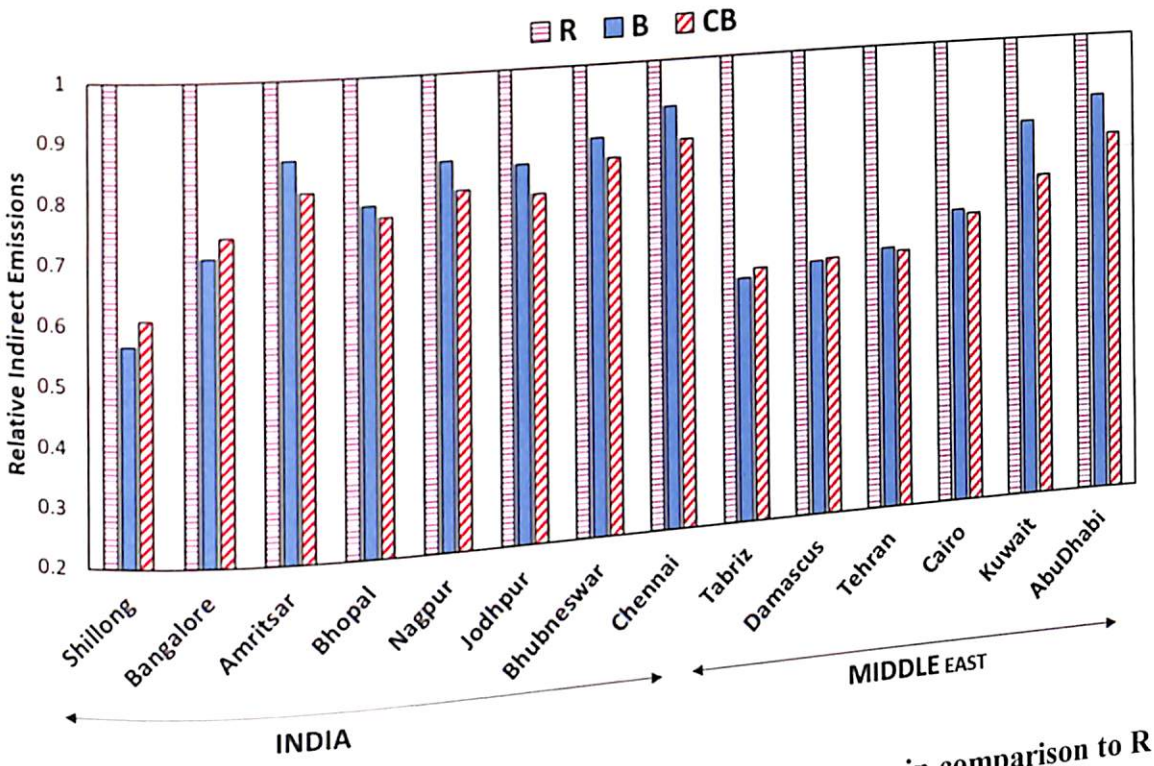

Fig. 6.30 Relative indirect emissions for B and CB configurations in comparison to R configuration

It is observable from Fig. 6.28, Fig. 6.29, Fig. 30 and Table 6.9 that the B configuration is a better solution in perspective of both energy consumption and emissions, for operation in Midlatitude climate in the Middle East and for the Cold and Temperature climate regions in India. While for the Dry Arid/Semi Arid climate in the Middle East and Composite, Warm Humid and Hot Dry regions in India, the CB configuration outperforms others. Compared to R configuration operating in Chennai, the reduction in total emissions for B and CB configurations are 41.1% and 44.9%, respectively. While the same is 46.3% and 49.6%, respectively, for operation in Jodhpur. Reduction in direct emissions dominates the share of total emissions reduction for both B and CB configurations. For example, the reduction in indirect emissions for B and CB configurations over R configuration for operation in Jodhpur is 17.1% and 21.9%, respectively. The performance of R, B and CB configurations in the Composite climate in India are not shown here, as there is no significant deviation.

Table 6.9 COP_{total} and Total Emissions ($TonsCO_{2equ}$) for R, B and CB configurations

MIDDLE EAST							
Climate	*Location*	*Annual avg. temperature (°C)*	*Annual average COP_{total}*			*Total Emissions ($kTonsCO_{2eq}$)*	
			R	*B*	*CB*	*R*	*B*	*CB*
ME1	Tabriz	12.15	3.18	*3.78*	3.68	19.26	*7.61*	7.80
	Damascus	16.69	3.02	*3.47*	3.45	19.23	*7.82*	7.86
ME2	Tehran	17.43	3.03	3.45	*3.48*	19.37	8.03	*7.96*
	Cairo	21.89	2.84	3.08	*3.12*	19.91	8.98	*8.88*
	Kuwait	26.63	2.46	2.49	*2.81*	22.17	12.11	*10.75*
	Abu Dhabi	27.31	2.55	2.58	*2.80*	23.21	13.25	*12.24*

INDIA							
Climate	*Location*	*Annual avg. temperature (°C)*	*Annual average COP_{total}*			*Total Emissions ($TonsCO_{2equ}$)×10^3*	
			R	*B*	*CB*	*R*	*B*	*CB*
IN1	Shillong	14.50	3.23	*3.90*	3.62	18.38	*6.67*	7.17
IN2	Bangalore	23.73	2.81	*3.09*	2.96	20.23	*9.19*	9.61
IN3	Bhopal	25.41	2.58	2.63	*2.80*	22.69	12.59	*11.80*
	Amritsar	27.57	2.68	2.81	*2.89*	21.28	10.71	*10.44*
IN4	Nagpur	26.95	2.60	2.66	*2.83*	22.41	12.23	*11.52*
	Jodhpur	26.20	2.62	2.69	*2.87*	22.12	11.87	*11.15*
IN5	Bhubaneswar	27.03	2.70	2.76	*2.88*	23.00	12.89	*12.36*
	Chennai	28.33	2.65	2.66	*2.85*	23.86	14.06	*13.16*

Fig. 6.31 and Fig. 6.32 visually illustrates the comparative advantage of the investigated systems in the various climatic regions, within map of Middle East and India, respectively. Fig. 6.33 presents the heating COP for the stand-alone R407C based system (SS) and integrated B and CB configurations, when operated in the month of January in a Midlatitude climate of Middle East and Cold climate of India. Both B and CB configurations depict similar heating COPs, at ambient temperature below 17°C for the major duration of January in Tabriz and Shillong. It is also observed that the heating COP for the SS is comparatively higher than B or CB configuration.

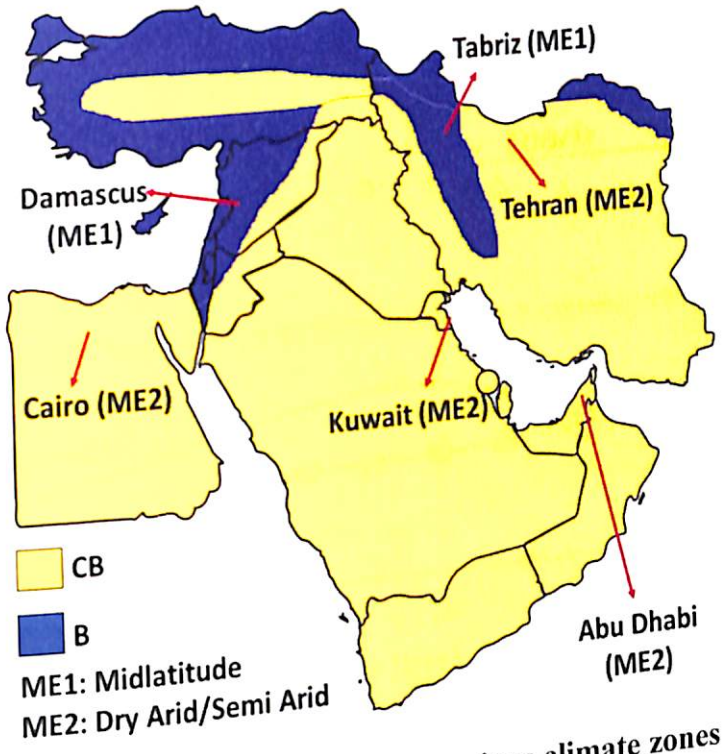

Fig. 6.31 Comparative advantage of systems in various climate zones of the Middle East

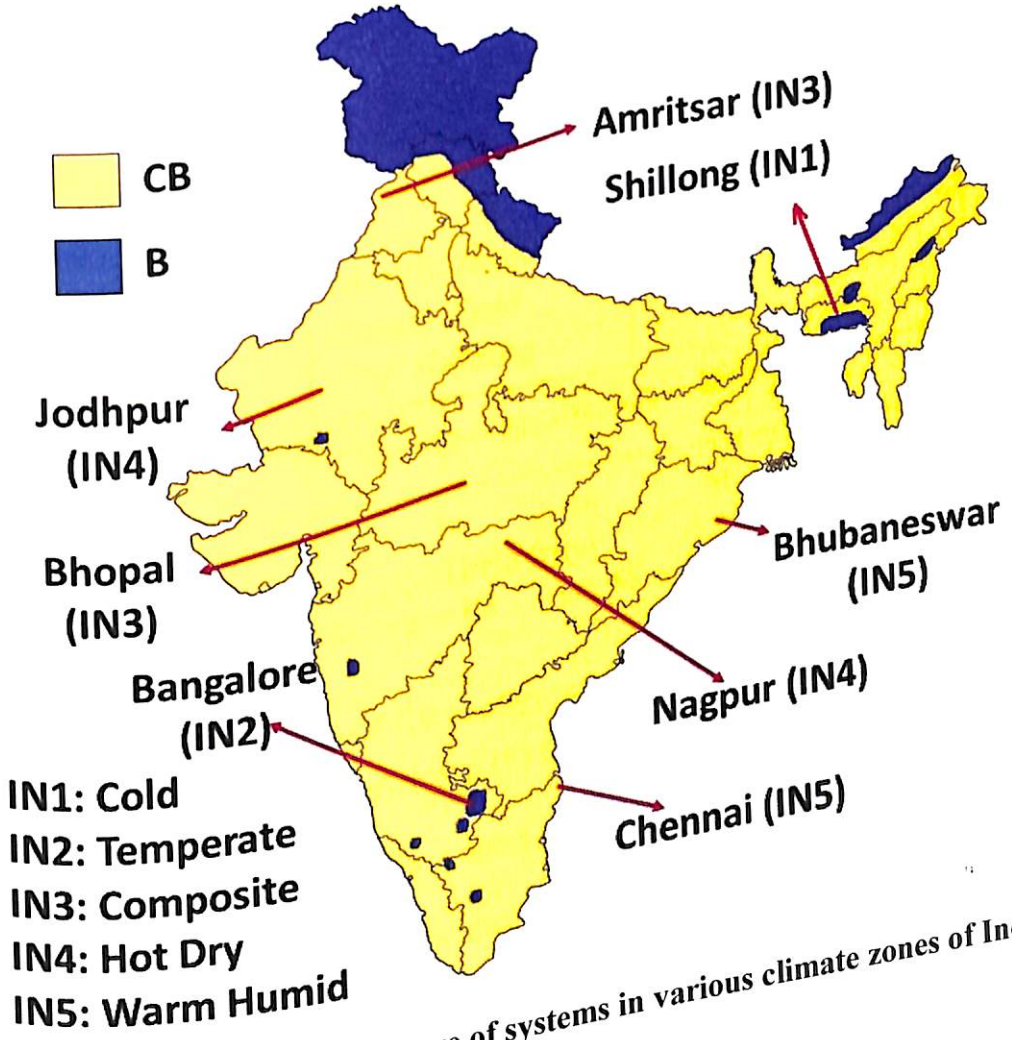

Fig. 6.32 Comparative advantage of systems in various climate zones of India

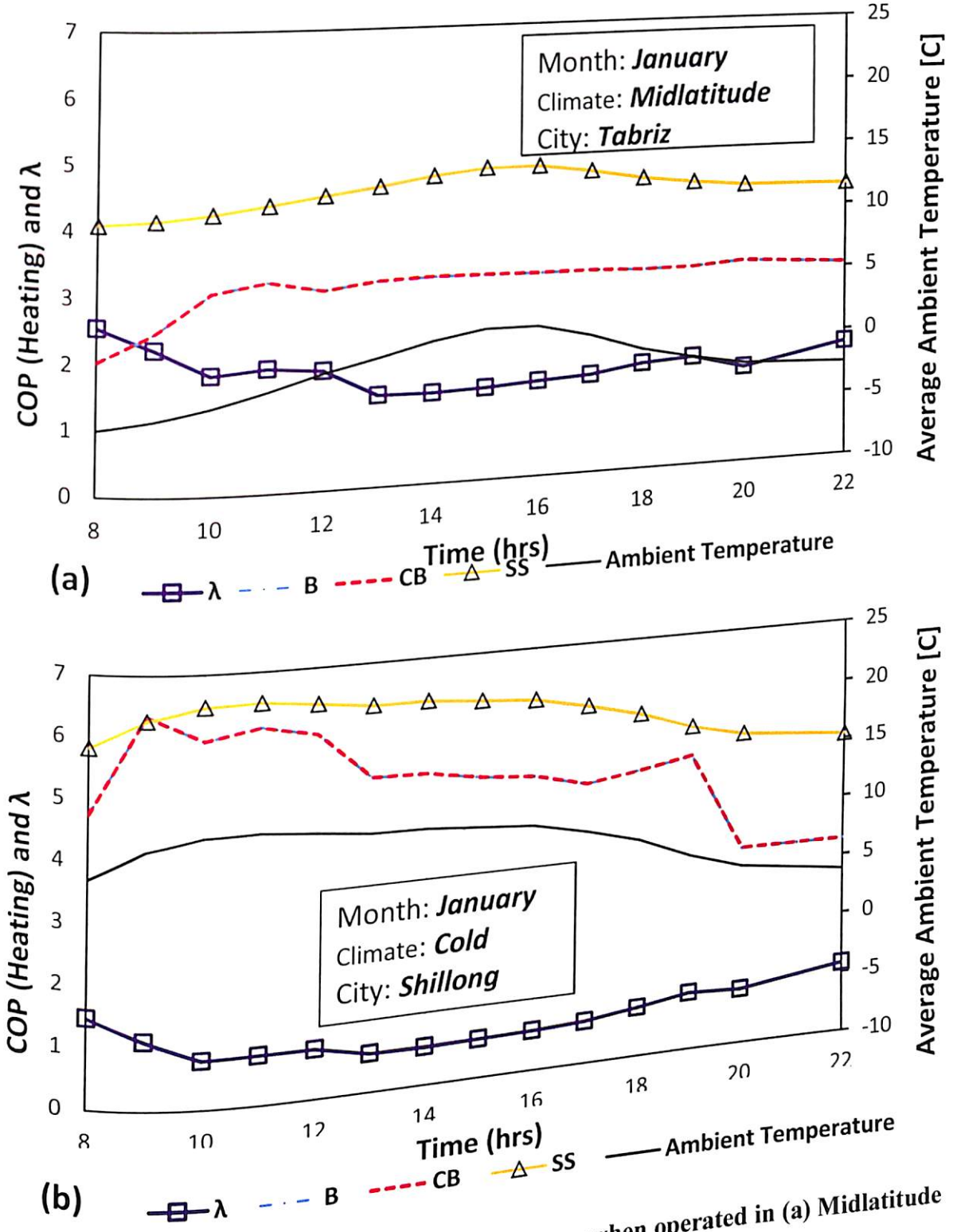

Fig. 6.33 Heating COP for B and CB configurations, when operated in (a) Midlatitude Climate (Tabriz) and (b) Cold Climate (Shillong)

Fig. 6.34 presents the COP for a stand-alone R410A based A/C system (SS) and the A/C integration in B and CB configurations, when operated in the month of June in a Dry

Arid/Semi-Arid climate of the Middle East (subplot (a), for Kuwait) and Hot Dry climate of India (subplot (b), for Jodhpur).

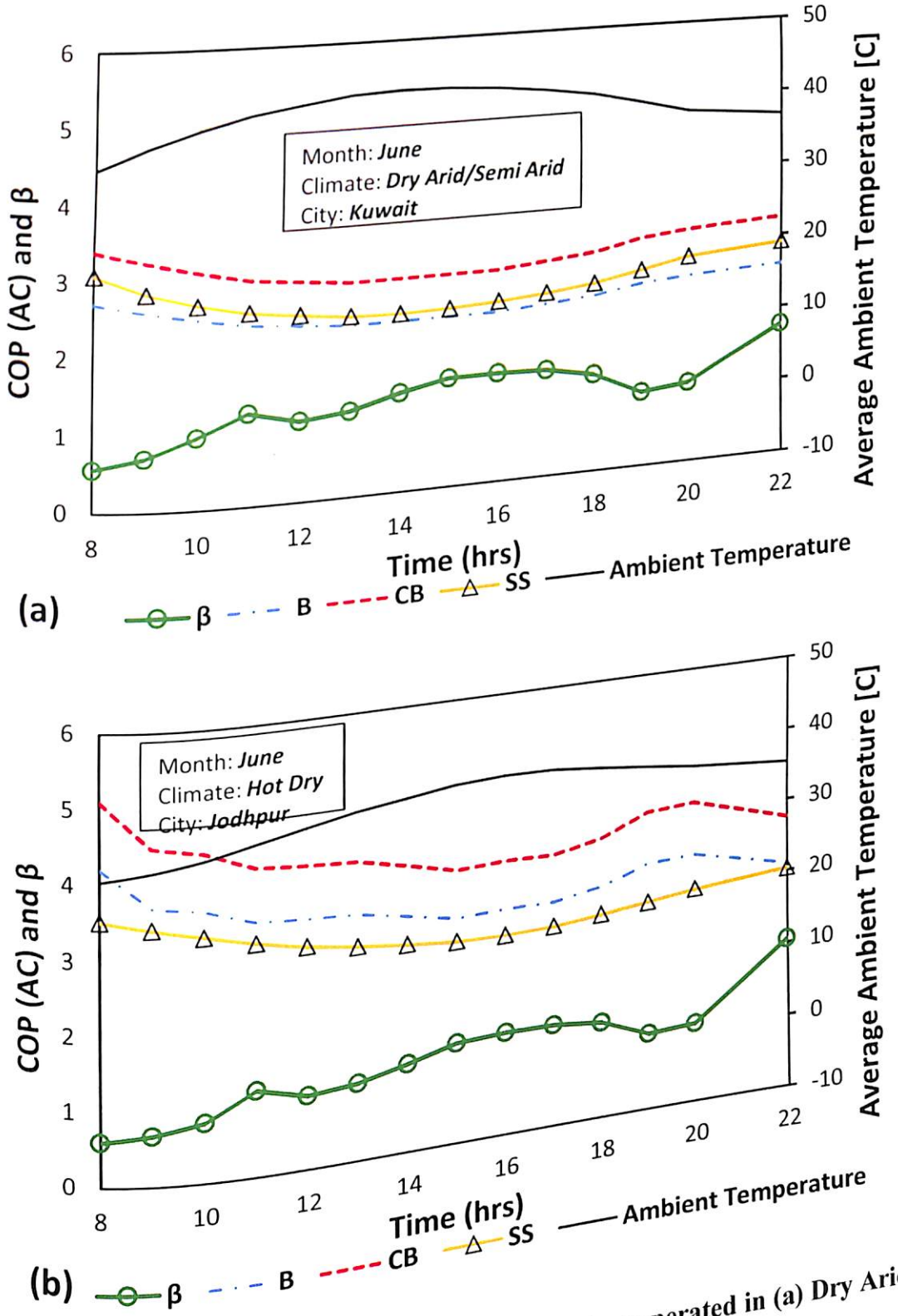

Fig. 6.34 COP of A/C in B and CB configurations, when operated in (a) Dry Arid/Semi Arid Climate (Kuwait) and (b) Hot Dry Climate (Jodhpur)

As observed from Fig. 6.34, the COP for the SS is comparatively lower. The difference, on an average is 12.58% and 36.4%, to that of CB configuration, for Kuwait and Jodhpur, respectively. The A/C COPs for CB and B configurations in Jodhpur are higher compared to that in Kuwait due to higher β values at comparatively lower ambient. Further, benefits associated with the environment friendly integrated A/C system are reduction in space and number of components required as well as ease of control.

The performance of CB configuration is sensitive to various assumptions made in this analysis. Among them, sensitivity of approach temperature of heat exchangers, minimum condensing temperature of R717 system and transition temperature of booster to cascade operation on overall system COP is investigated and the results obtained is plotted in a newly introduced Fig. 6.35. It is observable from Fig. 6.35 (a) that the COP of CB configuration increases by an average of 12% when the approach temperature of cascade condenser is decrease from 5 [K] (practical assumption taken in the current analysis) to hypothetical ideal value of 0 [K]. Whereas increasing the approach temperature from 5 [K] to 10 [K] leads to deterioration of performance by 13.5%. Similar behaviour is observed for system COP with change in approach temperature at condenser of R717 system leading to performance deterioration by 11.9% when the value is increased by 5 [K]. Fig. 6.35 (b) demonstrate the effect of minimum condensing temperature of R717 system on COP of CB configuration. With decrease in value for minimum condensing temperature there is a rise in overall COP. Sensitivity of COP of CB configuration with transition temperature of booster to cascade operation is presented in Fig. 6.35 (c). It is observed that optimization is required to select the appropriate transition temperature and based on the current assumptions made, transition temperature of 20°C is found to be optimum. The optimum transition temperature from booster to cascade configuration leads to minimum power consumption ensuring smooth transition as observed from Fig. 6.35 (c).

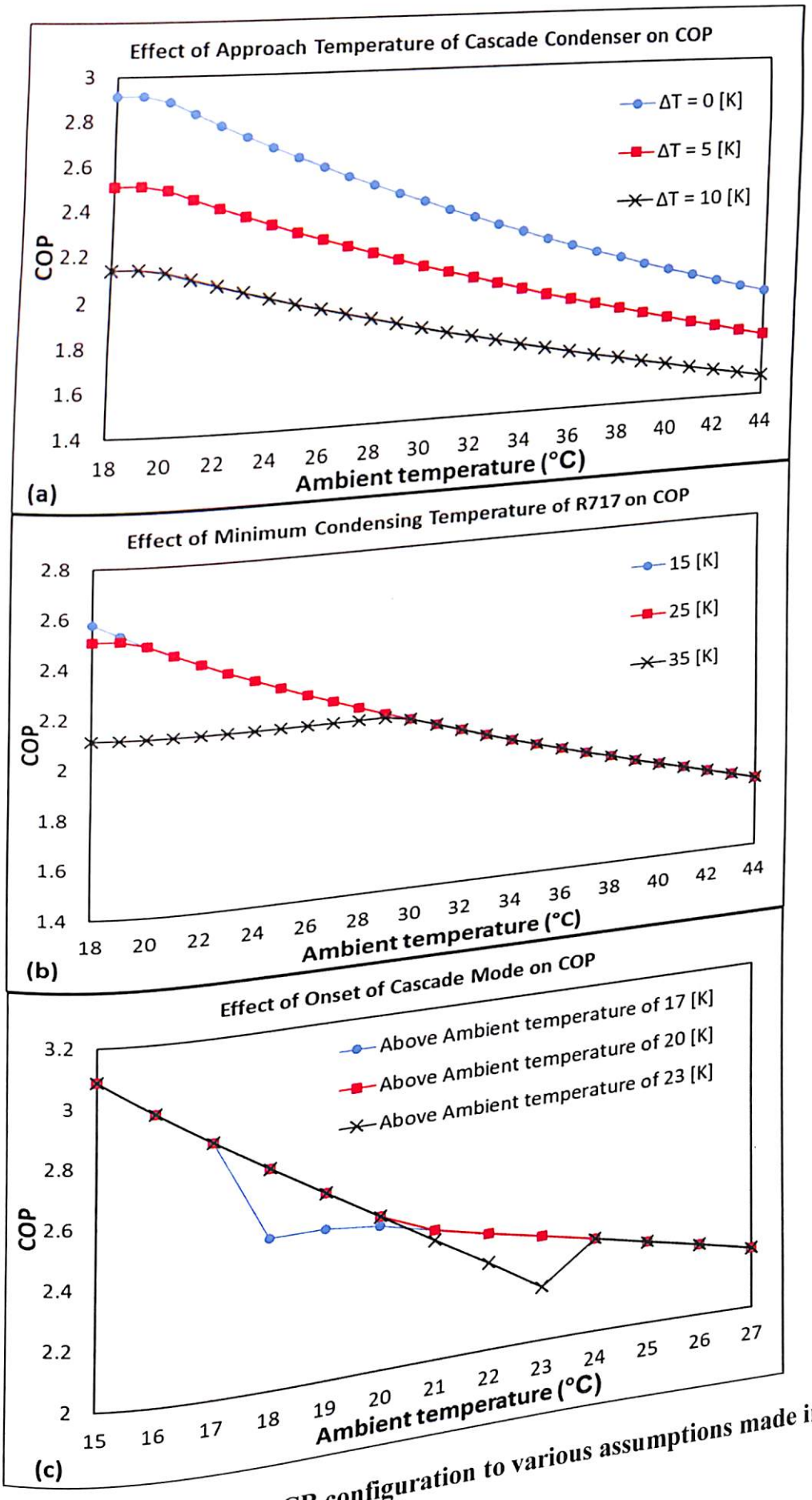

Fig. 6.35 Sensitivity of COP of CB configuration to various assumptions made in the analysis

6.3 Summary

In context to booster systems, B5 followed by B4, B3 and B2 are found to be better solution over B1 for entire range of investigation. Work recovery expander is found to have higher share in performance improvement of B5, followed by parallel compression. The difference in COP for system with and without flooded evaporator eventually decrease with increase in ambient temperature. The maximum energy savings for B5 over and above B1 is 22.16%, 15.2%, 20.06% and 16.8% when operated in New Delhi, Seville, Phoenix and Teheran respectively. The additional investment recovery time shows a non-linear trend with respect to local tariff for an isentropic efficiency. The slope of recovery time is steeper at lower tariff compared to that at higher. Indirect configurations (cascade) exhibits superior performance when operated in extreme warm climate of Delhi and Phoenix. While the performance of booster configuration equipped with parallel compressor is better when operated in mild climate of Seville and Teheran.

In context to integrated configurations, the simulation result reveals that the proposed CB configuration outperformance other systems while operating in extreme warm climate. In Kuwait (extreme warm climate), the annual COP_{total}, for CB configuration is better than the baseline (R), and B (all-CO_2) configurations by a maximum of 14.11% and 12.73%, respectively and the total emissions are lower by 51.5% and 11.2%. In Shillong (cold climate), the annual COP_{total} for the R, B and CB configurations are 3.23, 3.90 and 3.62, respectively. In comparison to the R configuration, the reduction in total emissions for the B and CB configurations are 63.7% and 61.1%, respectively. The heating COP for the stand-alone system (SS) is found higher by a maximum of 31.1% to that of the integrated configurations, while the COP for A/C is found higher for integrated cascaded booster (CB) configuration by a maximum of 36.4%.